Air Force Institute of Technology
AFIT Scholar

Theses and Dissertations | Student Graduate Works

3-23-2018

Impacts of Sub-Auroral Polarization Streams on High Frequency Operations as a Function of Modeled Particle Energy Flux

Nathan D. Smith

Follow this and additional works at: https://scholar.afit.edu/etd

Part of the Atmospheric Sciences Commons, and the Other Physics Commons

Recommended Citation
Smith, Nathan D., "Impacts of Sub-Auroral Polarization Streams on High Frequency Operations as a Function of Modeled Particle Energy Flux" (2018). *Theses and Dissertations*. 1756.
https://scholar.afit.edu/etd/1756

This Thesis is brought to you for free and open access by the Student Graduate Works at AFIT Scholar. It has been accepted for inclusion in Theses and Dissertations by an authorized administrator of AFIT Scholar. For more information, please contact richard.mansfield@afit.edu.

IMPACTS OF SUB-AURORAL POLARIZATION STREAMS ON HIGH FREQUENCY OPERATIONS AS A FUNCTION OF MODELED PARTICLE ENERGY FLUX

THESIS

Nathan D. Smith, Captain, USAF

AFIT-ENP-MS-18-M-097

DEPARTMENT OF THE AIR FORCE
AIR UNIVERSITY

AIR FORCE INSTITUTE OF TECHNOLOGY

Wright-Patterson Air Force Base, Ohio

APPROVED FOR PUBLIC RELEASE; DISTRIBUTION UNLIMITED

The views expressed in this thesis are those of the author and do not reflect the official policy or position of the United States Air Force, Department of Defense, or the United States Government. This material is declared a work of the U.S. Government and is not subject to copyright protection in the United States.

AFIT-ENP-MS-18-M-097

IMPACTS OF SUB-AURORAL POLARIZATION STREAMS ON HIGH FREQUENCY OPERATIONS AS A FUNCTION OF MODELED PARTICLE ENERGY FLUX

THESIS

Presented to the Faculty

Department of Engineering Physics

Graduate School of Engineering and Management

Air Force Institute of Technology

Air University

Air Education and Training Command

In Partial Fulfillment of the Requirements for the

Degree of Master of Science in Applied Physics

Nathan D. Smith, BS

Captain, USAF

March 2018

DISTRIBUTION STATEMENT A.

APPROVED FOR PUBLIC RELEASE; DISTRIBUTION UNLIMITED

AFIT-ENP-MS-18-M-097

IMPACTS OF SUB-AURORAL POLARIZATION STREAMS ON HIGH FREQUENCY OPERATIONS AS A FUNCTION OF MODELED PARTICLE ENERGY FLUX

Nathan D. Smith, BS

Captain, USAF

Committee Membership:

Robert D. Loper, PhD
Chair

Maj Omar A. Nava, PhD
Member

Maj Daniel J. Emmons, PhD
Member

Abstract

Space weather events can cause irregularities within the ionosphere; in particular, this research examines sub-auroral polarization streams (SAPS), as their accompanying irregularities and effects can degrade high-frequency (HF) signal propagation. It is known that the strongest westerly current drifts delineating SAPS are associated with a deep ionospheric trough, which in turn contaminates HF data with clutter from the non-standard ionosphere. Having a methodology to track and identify these occurrences on current computational architecture would provide operators enhanced situational awareness in knowing to expect degradation in HF processes. This study has discovered a weak, yet significant, exponentially decaying correlation between maximum SAPS flow velocity and electron energy flux. Also examined is overarching characteristics most commonly associated with SAPS events. It has been noted that March is the most common month for SAPS formation, as well as finding electron energy flux for SAPS flow to be 4.0 ergs/cm^2s with a the best regression analysis (R^2 value) during solar minimum, indicating electron energy flux is the best parameter to use when locating SAPS. The location of the energy flux is just as important, if not more, than locating the proper energy flux values. This information established an operational rule of thumb to help radar operators determine when SAPS events will degrade standard radar operations.

Acknowledgments

I would like to express my sincere appreciation to my faculty advisors, Dr. Robert Loper, Maj Omar Nava, Maj Daniel Emmons for their guidance and support throughout the course of this thesis effort. The insight and experience was certainly appreciated. I would, also, like to thank the University of Calgary, as well as the Department of Electrical and Computer Engineering at Virginia Polytechnic Institute and State University (VA Tech) for their collaborative information sharing and access to data. Simulation results have been provided by the Community Coordinated Modeling Center (CCMC) at Goddard Space Flight Center through their public Runs on Request system (http://ccmc.gsfc.nasa.gov). The OVATION Prime Model was developed at Johns Hopkins University Applied Physics Laboratory. Finally, I would be remiss to not thank my supporting wife and loving family for all they have done and sacrificed for me during this endeavor.

Nathan D. Smith

Table of Contents

Page

List of Figures

List of Tables

Page

1 Introduction

1.1 General Issue

Radio Detection And Ranging (radar) systems are used to detect the presence, direction, distance, and speed of aircrafts, ships and weather phenomena by transmitting short duration pulses of high-frequency (HF) electromagnetic radiation that are backscattered by the target. These reflected signals are received by the radar during breaks between transmissions, and from that received information trained operators can determine characteristics of the target. There are operations, both military and non-military, which use radio-wave information from radar systems that often provide situational awareness of natural or man-made objects. Line-of-sight radar systems have an innate problem: the bend of the Earth's surface. The maximum range of these radars is limited by the radio horizon. Over-the-Horizon radars (OTHR) capitalize on the ionospheric reflection by transmitting sky-waves to increase the effective range to upwards of 5,000 kilometers. Sky-wave propagation uses HF shortwave radio frequencies. The neutral atmosphere is transparent to radio waves in this part of the electromagnetic (EM) spectrum. As a result, they will propagate unimpeded up to the top of the atmosphere until they are reflected off ionospheric plasma. Given certain conditions, radio signals transmitted at an angle into the sky will be reflected back towards the ground by the ionosphere, allowing them to return to earth beyond the radio horizon. A small amount of this signal will scatter off the desired targets back towards the sky, reflect off of the ionosphere again, and return to the receiving antenna by the same path (Headrick 1998). There is only a narrow band that exhibits this bounce behavior: the HF spectrum of 3-30 MHz. Because the optimal

frequency depends on current conditions of electron densities, sky-wave systems utilize real-time monitoring of the ionosphere to continuously adjust the frequency of the transmitted signal (Reinisch 1997).

Past research into Sub-Auroral Polarization Streams **(**SAPS) has largely focused on understanding and characterizing the phenomena rather than developing ways to evaluate its occurrence and impacts. The operational impact of SAPS to high frequency electromagnetic signals has not been fully investigated. It has been found that the maximum SAPS flow is associated with a deep plasma density trough (Foster 2002). This density trough can impede radar operations by lowering the plasma density, forcing the radar operate at its lowest frequency range, which may still be too high of frequency to be refracted back to earth, allowing for signal escape as shown in Figure 1. Further, the trough can introduce ionospheric clutter (Figure 1), as well as lead to severe off-great-circle propagation (Dandekar 1995). Accurate use of HF data requires knowledge of where and when troughs occur; there needs to be an operational way to identify these events without relying on real-time monitoring. The operational tool that the Air Force employs is the Oval Variation, Assessment, Tracking, Intensity, and Online Nowcasting (OVATION) Prime model which tracks and models the ionospheric conditions within the auroral zone using real-time solar wind data. Because particles that contribute to the initiation of SAPS originate from within the Ring Current this research intends to correlate modelled particles energy and observed locations of SAPS occurrences in order to mitigate operational effects and impacts triggered by the ionospheric anomalies.

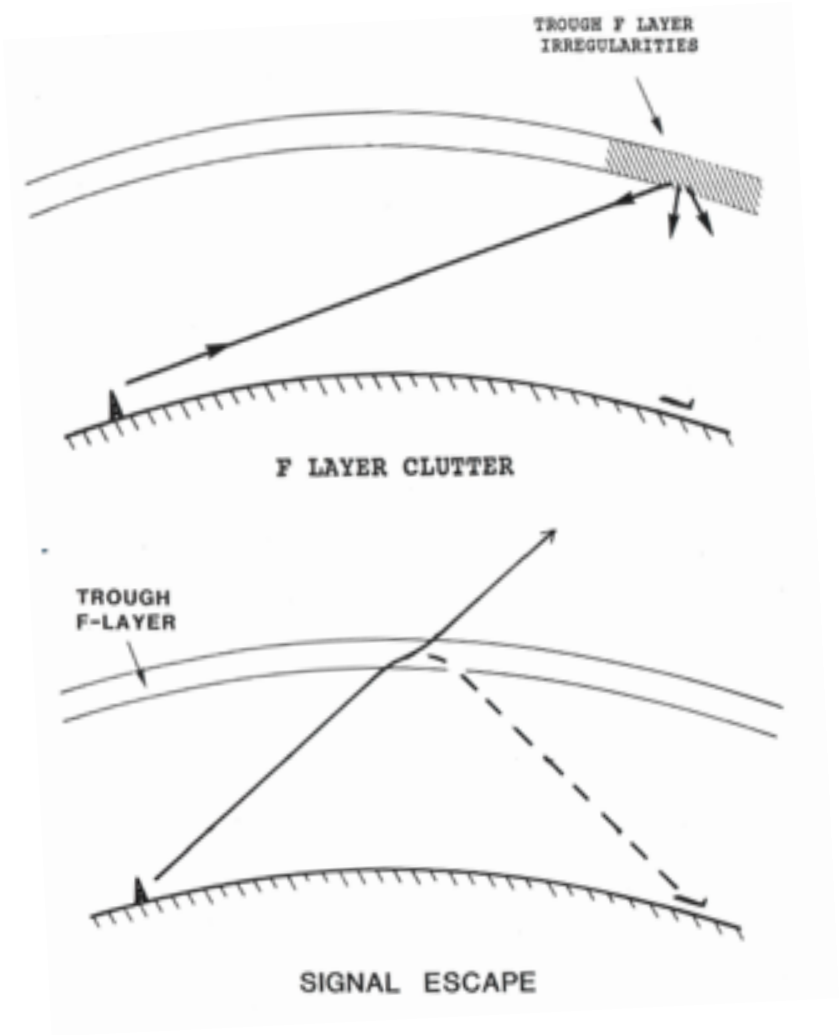

Figure 1 Impacts of Ionospheric Trough (Dandekar 1995)

Schematic example of F layer irregularities that may scatter radar signals, producing clutter at range of target before detection. Also depicted is an example of transmitted HF signal escaping to space because it has too high of a frequency to be refracted back to Earth by an F layer low density trough.

1.2 Problem Statement

Both civilian and military operations operate high-frequency (HF) radio signals in order to exploit ionospheric reflections to propagate transmissions to long ranges. The ionosphere acts as a dynamic mirror that varies diurnally, seasonally, and with the solar cycle. Properly utilizing an ionospheric reflection requires specific knowledge of ionospheric conditions to correctly interpret the data. There are multiple space weather events that can cause irregularities within the ionosphere, specifically of interest, is the sub-auroral polarization streams (SAPS) as its effects has not been fully examined. It is known that the strongest westerly current drifts delineating SAPS are associated with a deep ionospheric trough (Foster and Vo, 2002), which in turn, contaminates data with clutter from the non-standard ionosphere (Dandekar 1995). Having a methodology to track and identify these occurrences would provide operators enhanced situational awareness in knowing to expect degradation in HF processes. There are currently procedures in place to assess space weather effects on radar operations, but no extensive work has been done to discover SAPS impacts. It is important to find innovative ways that allows radar operators to detect SAPS impacts without having to rely on real-time ionospheric data to improve upon operational success. SuperDARN radar and modelled particle energy fluctuations are used in hopes to find an operational correlation between the two in order to circumvent using real-time ionospheric sampling methods.

1.3 Research Objectives/Hypotheses

The research objective of this thesis is to determine a parameter within current operational architecture that will allow space weather technicians to nowcast HF impacts associated with SAPS without relying on real-time ionospheric measurements. It is suspected there will be a correlation between the particle energies (be it electron energy, ion energy, or both) to the known location of SAPS. It is hypothesized that the faster westward plasma flow associated with a SAPS event will be associated with higher particle energy flux values, while the slower plasma flows will be associated with lower flux values. It is also speculated that the best parameter to use for SAPS location identification will be electron energy fluctuations, as electron number density is the main focus of space weather impacts within the ionosphere.

1.4 Investigative Questions

1. What are the existing abilities by which SAPS are detected and measured? How can those methods be improved?
2. Can the existing space weather technology and forecast methods be adapted or modified to capture SAPS events or associated impacts?
3. How will OVATION Prime handle modeling space weather at lower latitudes? Is there a specific limit?
4. How far equatorward do SAPS typically occur? (How sub-auroral)
5. Is there a temporal dependence on SAPS? (i.e. Seasonal? Part of solar cycle?)
6. Under what conditions can SAPS best be detected in OVATION Prime?

7. How much can HF operations be improved upon by identifying SAPS events? Is knowing enough?

1.5 Methodology

First, the SAPS event must be detected and tracked on ionospheric radars such as SuperDARN. Information from the radar will be used to calculate basic parameters and characteristics of each SAPS occurrence. Parameters include, but are not limited to: year, month, day, time SAPS began and ended, time of peak flow, max and min latitude of occurrence, and magnetic local time of event. From this, a database is established and used to examine trends. Secondly, the OVATION Prime model is used to provide information on particle energy fluctuation values. The time and location from the SAPS database is then used to track where the streamer is occurring and the coordinates are tracked in OVATION Prime to log flux values on each event. Flux data is then analyzed both by common occurrence as well as a function of SAPS flow speed to uncover any relationship that exists. Finally, the correlations are used to create forecasting methods in order to use existing architecture to predict clutter and signal fading impacts to HF operations.

1.6 Assumptions/Limitations

This project will examine 87 SAPS events during a 5-year period, from December 2007 to April 2013. Solar cycle 24 began in December 2008 and reached its peak in April 2014. Data captures the waning portion of cycle 23 and into the upswing from solar minimum towards solar maximum of cycle 24. Each SAPS occurrence has to be detected from radar data over two consecutive scans to locate, track, and calculate the movement

and velocity of the westward streamer. The occurrence of the streamer must then be tracked in the OVATION Prime model, finding its location as best as possible due to the models resolution and determine particle energies, again limited to model resolution and output scaling bins. The OVATION Prime model, while determined to be the most accurate model (Lane 2012), will still carry innate limitations. It is not a full depiction of what is truly happening across the entire ionosphere, nor does it encapsulate the full range of space weather dynamics and atmospheric electrodynamics. Furthermore, no studies have been conducted to determine the effectiveness of OVATION Prime in the sub-auroral latitudes. OVATION Prime's output display includes the poles and extends equatorward to roughly 45 degrees latitude, which encapsulates all of the SAPS' latitude of max flow in all identified occurrences. Also, SuperDARN is a line-of-sight radar whose beamwidth increases with altitude the further the target is away from the radar. This study will assume all recognized SAPS streamers occur at the same altitude occurring in a plane-parallel atmosphere. Additionally, all data captured has been recorded solely in the Northern Hemisphere. Huang and Foster (2007) found SAPS to occur as magnetic conjugates, ergo this thesis assumes the Southern Hemisphere behaves in the same manner as the Northern Hemisphere. The final assumption is space weather nowcasting methods uncovered by this study will enable trained radar operators and imagery analysts to recognized SAPS flow streamers by identifying patterns in particle energy flux output values from OVATION Prime.

2 Background

2.1 Chapter Overview

The purpose of this chapter is to first provide background information on the source of space weather, explain how the earth's atmosphere responds and outline the processes that generate SAPS events. Next examined will be real-time radar ionospheric sampling as well as how space weather technicians utilize solar wind data to make predictions.

2.2 Ionosphere

Earth's atmosphere acts as a shield for hazardous solar radiation by absorbing the most energetic photons, specifically extreme ultraviolet and x-rays. These photons contain sufficient energy to overcome the binding energy of neutral atmospheric constituents to dislodge an electron upon absorption (Gurnett 2005). This atmospheric photoionization causes the planet to be surrounded in a plasma known as the ionosphere. The ionosphere typically starts around 80 kilometers in altitude during the day and extends upwards to 1000 kilometers above the earth. During the night, when there is no incoming solar radiation, cosmic rays are able to continue ionizing particles, however not nearly as strongly as the Sun (Schunk 1976). Thus, the ionosphere is much less charged during nighttime, allowing for the lower levels to vanish until sunrise. The ionosphere is classified into four layers based upon electron density peaks: the F2, F1, E and D region (Figure 2). The electron density is highest in the F2 region, with the greatest concentration occurs around 300 kilometers, while the D region is the lowest in altitude and electron concentration.

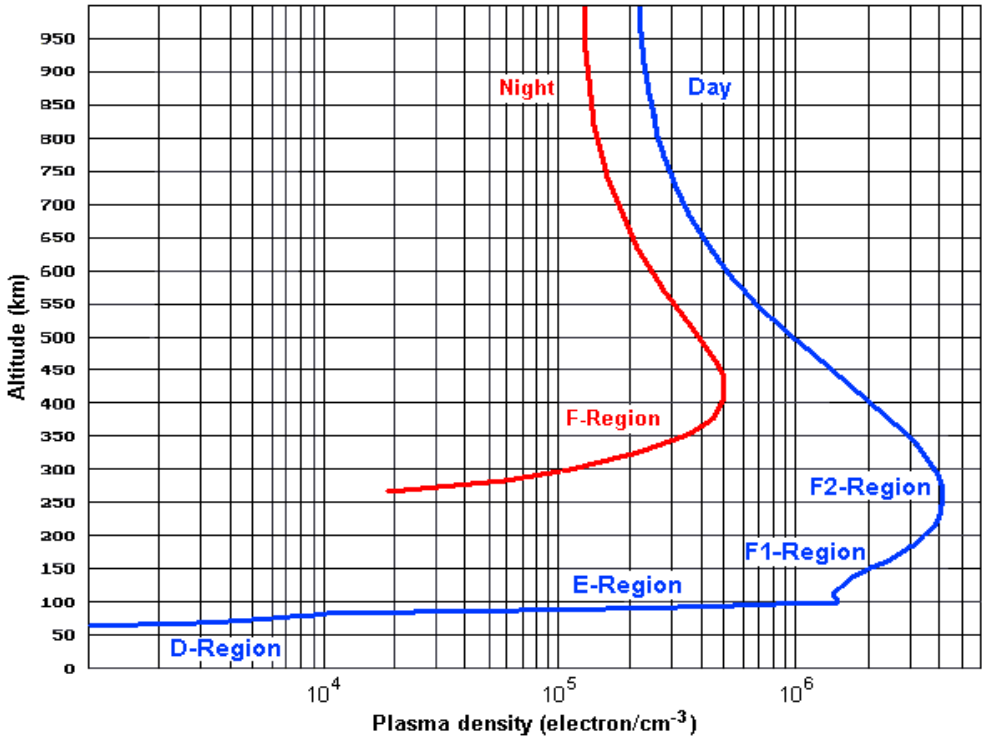

Figure 2 Ionospheric Plasma Density (UC Berkley)
Structure of ionosphere layers based upon total electron number density. The different layers are based upon local maxima in the number density. The blue line shows the ionosphere structure during the day while the red line shows the lower portions of the ionosphere vanishing at night and being replaced by a higher altitude F region. Credit: Bob Brown, U.C. Berkley

2.3 Plasma Frequency

The electron plasma frequency is the natural frequency of oscillation of electrons in a plasma that are displaced relative to the ion background (Gurnett 2005). For a radio wave to reflect off the atmospheric plasma, the wave must have a frequency less than the electron plasma frequency. The equation for the plasma frequency is given by:

$$f_{pe} = \frac{1}{2\pi}\sqrt{\frac{n_e e^2}{\epsilon_0 m_e}} \approx 8.979\sqrt{n_e}, \quad (1)$$

where:

f_{pe}= electron plasma frequency, kHz

m_e= mass of an electron, kg

n_e= electron number density, cm^{-3}

e^2= elementary charge (charge of an electron), C

ϵ_0= permittivity of free space, $kg^{-1}m^{-3}s^4A^2$

Equation 1 contains mostly physical constants, therefore, depicting the electron plasma frequency is dependent upon the electron number density within the ionosphere. Selecting the correct frequency to achieve the ionospheric reflection can be challenging. The differing layers of the ionosphere will each have separate plasma frequencies as the number density changes. Electron number density is also highly variable, depending upon: solar activity, composition of the neutral atmosphere, time of day, time of year, geographic location as well as electron interactions with the geomagnetic field and atmospheric electrodynamics.

The lowest range of the plasma frequency comes from the D layer. Using values from the standard ionosphere (Figure 2) the electron number density in this region is on the order of 10^9 $electrons/m^3$. By plugging in this value, the plasma frequency is 0.3 MHz. The highest range of the plasma frequency comes from the daytime F2 region. Here, the electron number density during a standard atmosphere (Figure 2) is on the order of 2 x 10^{12} $electrons/m^3$. With this number density, the plasma frequency is 12.7 MHz. During space weather events, the F2 region can deviate from standard atmosphere, greatly increasing the electron density due to more ionization energy injected into the atmosphere from solar flares. The increases density allows for a higher usable maximum frequency.

The calculated plasma frequencies show HF signals radio waves in the range of 3-30 MHz are required for the ionospheric reflective bounce to occur.

2.4 Space Weather and Solar Activity

Space weather is a branch of space physics that focuses on the time varying conditions of the solar wind and its resulting impacts to the space environment surrounding Earth, to include conditions within the ionosphere and magnetosphere—the region above the ionosphere surrounding the earth, in which magnetized plasma motion is controlled by the earth's magnetic field (Poppe 2006). The Sun is the main driving force of all space weather events; within the Solar System, it is influenced by the solar wind and the interplanetary magnetic field (IMF) associated with the solar plasma. A variety of physical phenomena are associated with space weather including: solar flares, geomagnetic storms and substorms, energization of the Van Allen radiation belts, Coronal Mass Ejections (CME), energetic proton events, and Sudden Ionospheric Disturbances (SID). SID are connected to abnormally high plasma densities in the lower ionosphere caused by increased ionization due to solar flares. SID result in a sudden increase in radio-wave absorption causing complete blackout of radio communications, known as short wave fading, which can last for minutes to hours (Pisacane 2008). Solar flares and CMEs can compress the daytime magnetosphere causing deviations in the baseline geomagnetic fields

Space weather is monitored by ground measurements alongside spacecraft measurements by observing changes in the Earth's magnetic field over periods of time, ranging from seconds to days. There are several indices to quantify these magnetic changes, however this study will focus on the Kp index. First, the K index quantifies

disturbances in the horizontal component of earth's magnetic field with an integer number, ranging from zero to nine (0-9), with 1 being calm (Table 1), and 5 or more indicating geomagnetic storming. The K index is derived from the maximum fluctuations of horizontal components observed on a magnetometer during a three-hour interval (Pisacane 2008). Next is the Kp index which is derived by calculating a weighted average of K indices from 13 predetermined geomagnetic observatories stations (Pisacane 2008). The subscript *p* denotes a planetary value that smooths out longitude dependence by averaging global measurements.

Kp Index	0-2	3	4	5	6	7-9
Storming Condition	Quiet (Calm)	Unsettled	Active	Minor Storming	Major Storming	Severe Storm

Table 1 Kp Index and Associated Storming Conditions

2.5 Atmospheric Conductivity

The interaction between electrically charged particles in a magnetic field plays a key role in SAPS formation. SAPS flow is strongly driven by the electric drift, often called the $\vec{E} \times \vec{B}$ drift. This drift is generated by an electric force perpendicular to the magnetic field in which the charge dependence mathematically cancels out, allowing both ions and electrons drift in the same direction, unlike particle drifts driven by other external forces. Forces on the plasma such as atmospheric pressure gradients, neutral winds, and geomagnetic fields cause both ions and electrons to drift and move separately within the atmosphere causing a charge separation. This, in turn, drives an atmospheric current. These

currents cause greater charge separation and charge build up which generates an electric field to counteract the built up charge. This is a key process in SAPS generation. The extent and strength of these currents are related to external forces through atmospheric conductivity—the measure of the gas's ability to conduct current. The governing equation for the currents is given by:

$$\vec{J} = \overleftrightarrow{\sigma} \cdot (\vec{E} + \vec{u}_n \times \vec{B}) \qquad (2)$$

Where:

$\vec{J}$ = electric currents, A

$\overleftrightarrow{\sigma}$ = conductivity tensor, mhos

$\vec{E}$ = electric field, V

$\vec{u}_n$ = neutral wind , m/s

$\vec{B}$ = geomagnetic field, T

Figure 3 depicts how the strength of conductivity changes drastically within the ionosphere. At low altitudes (below 100 km), electron density is small and the collisional rate is large so the conductivity approaches zero. In mid altitudes electron density increases as the collisional rate decreases making the conductivity increase rapidly, while at high altitudes (300 km and up) both the electron density and collisional rate decreases making the conductivity more like a constant. The equation for isotropic conductivity is given by a scalar quantity:

$$\sigma = \frac{n_s\, q_s^2}{m_s\, \nu_{sn}} \qquad (3)$$

Where:

σ = conductivity, mhos

n_s = number density of species, m^3

q_s = charge of the species, elemental charge (particle dependent)

m_s = mass of the species, kg

ν_{sn} = collisional rate of the species with neutral particles, s^{-1}

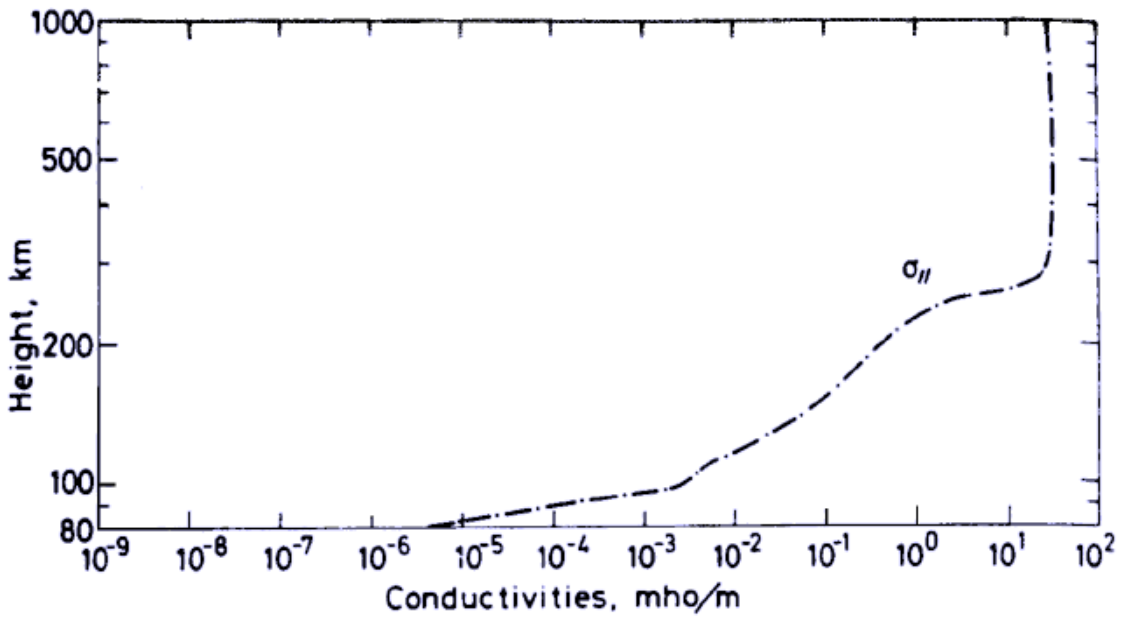

Figure 3 Conductivity vs Altitude (Kelley 2009)
Atmospheric scalar conductivity as a function of height (Kelley 2009)

2.6 Magnetic Local Time

Geospace phenomena such as the aurora, plasma motion, and ionospheric currents are organized by the Earth's main magnetic field. Solar wind plasma can move relatively freely along geomagnetic field lines, however particles cannot move across them unless

acted on by an external force. Due to this constraint, it is helpful to present these phenomena in a coordinate system relative to the Earth's intrinsic magnetic field. The coordinate system used in this study is known as Magnetic Local Time (MLT). This coordinate system maps data with respect to the position of the Sun-Earth alignment. MLT places the Sunward facing portion of the earth, the subsolar point, (daytime) at 12 noon, while the portion 180 degrees rotated from the subsolar point (nighttime) is plotted as 00 midnight (Figure 4). The section of the earth that is about to experience sunrise (dawn) is plotted at 06 while the section of the earth is about to experience sunset (dusk) is plotted at 18 (Laundal 2014).

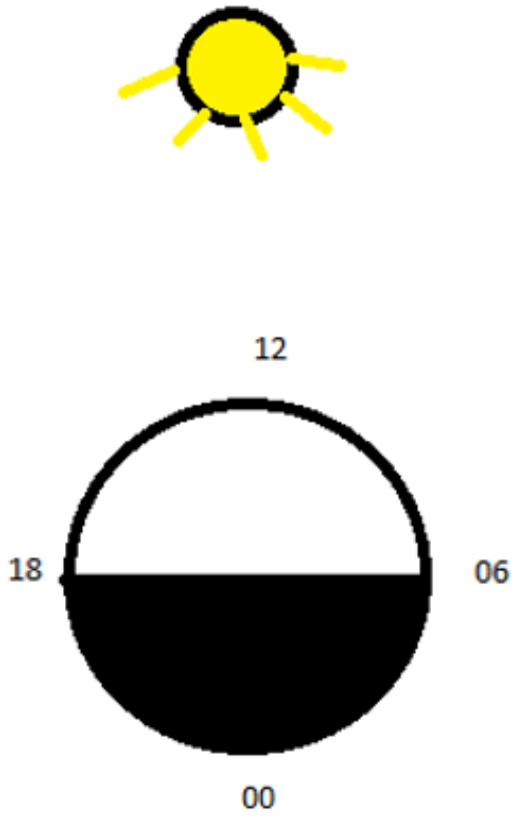

Figure 4 Magnetic Local Time Schematic
The subsolar point, 12, directly faces the sun while the most antisunward point is plotted as 00. 06 represents the dawn portion, while 18 represents the dusk sector.

2.7 McIlwain Parameter

The McIlwain parameter, commonly referred to as the L-shell or L value, is a parameter describing a particular set of planetary magnetic field lines. Typically, along the equator, the L-shell often describes the set of magnetic field lines which cross the Earth's magnetic equator at a number of Earth-radii equal to the McIlwain parameter (Pisacane 2008). For example, L=2 describes the set of geomagnetic field lines which cross the magnetic equator two earth radii from the center of the earth. At the equator, an L-shell

value of 1 coincides with Earth's surface. The L-shell is often used to give a general picture of magnetic phenomena near Earth using the dipole model of Earth's magnetic field (Figure 5). In a centered dipole approximation, the path along any given L-shell can be described by Equation 4.

$$r = L\cos^2\lambda \tag{4}$$

Where:

r = radial distance in earth radii to a point on the field line

L = the L-shell of interest, $L \equiv \frac{r}{R_{earth}}$ when $\lambda = 0$

$\lambda =$ geomagnetic latitude, degrees

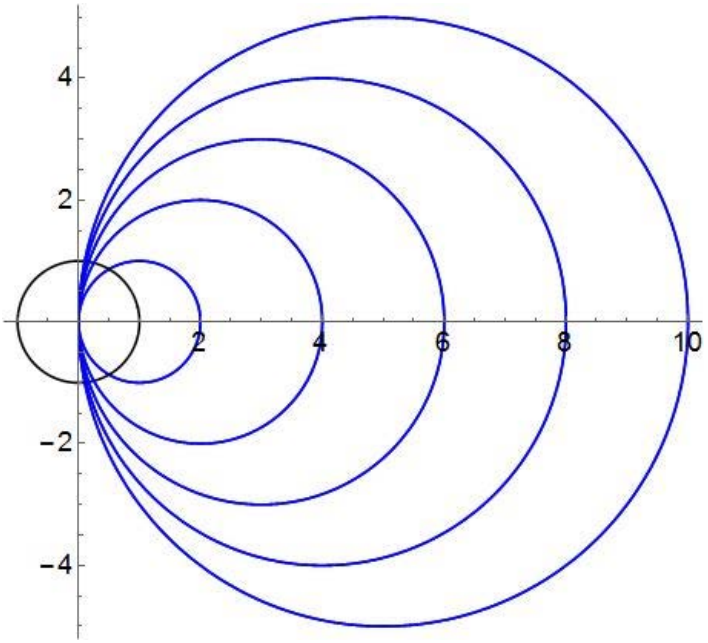

Figure 5 L-Shell Isopleths

L-shell values for geomagnetic field lines extending out to 10 earth radii. Note how the field lines converge near the poles. Here, the distances are not a full earth radii due to the factor of $\cos^2\lambda$

2.8 Sub-Auroral Polarization Streams

The basic processes of the SAPS flow is now well understood; Anderson et al. (1993) proposed a production mechanism for SAPS flows as an establishment of poleward sub-auroral electric field through closure of region-2 field-aligned currents (R2 FACs) in the low-conductivity sub-auroral ionosphere. In the pre-midnight region, R2 FACs flow into the ionosphere at lower latitudes (downward FAC) and towards the magnetosphere at higher latitudes (upward FAC). To keep ionospheric current continuity, these FACs close through a poleward-directed Pedersen current, which is associated with a poleward-directed electric field that gives westward drifts and reduction of the electron density known as the plasma trough (Schunk et al., 1976). Foster (2002) termed this enhanced westward flow as the Sub-Auroral Polarization Stream. Foster and Vo (2002) found the average characteristics of SAPS from two solar cycles, 1979-2000, to be a persistent secondary westward convection peak which lies equatorward of the auroral two-cell convection. They also note that SAPS span the nightside from dusk to the early morning sector for all K_p greater than 4. In the pre-midnight sector, the SAPS westward convection lies equatorward of L-shell equal to 4 (60 degrees invariant latitude) spans 3–5 degrees of latitude, and has an average peak amplitude of more than 900 m/s. In the predawn sector, SAPS is seen as a region of anti-sunward convection equatorward of L-shell equal to 3 (55 invariant latitude) spanning approximately 3 degrees of latitude with an average peak amplitude of 400 m/s.

Ionospheric currents play a critical part in linking the ionosphere to the magnetosphere by energizing ring current ions within the Van Allen radiation belt, as well

as conducting thermal plasma in the inner magnetosphere and mid-latitude ionosphere (Foster 2002). Currents driven into the sub-auroral ionosphere from the disturbed ring current trigger a sequence of magnetosphere-ionosphere coupling with dramatic consequences for the electric field. During geomagnetic storms, the electric fields and particle populations that define the auroral zone (60 degrees latitude and poleward) expand equatorward (extent depends on strength of geomagnetic storming) and the effects are felt at previously sub-auroral latitudes (45 degrees latitude) (Foster and Vo 2002). These night-sector enhanced convection patterns deviate from the Volland-Stern two-cell pattern (Figure 7). The generalized, inclusive term for these ionosphere-magnetosphere linking electrodynamic currents phenomena is Sub-Auroral Polarization Streams (SAPS) (Foster 2002). It is important to note that the term SAPS denotes the electric fields and the mechanisms that drive them, not their effects on the atmosphere (Foster 2002).

Electric fields often appear in regions of low ionospheric conductivity equatorward of auroral electron precipitation. Galperin (1974) first reported polarization jets (PJ) as strong, polewardly directed electric fields driving sunward plasma convection at sub-auroral latitudes in the local evening sector. Similar intense, narrow structures are typically referred to as sub-auroral ion drifts, (SAID) as coined by Spiro (1979). Yeh (1991) noted a broader region of sunward plasma drift that is equatorward of the evening auroral convection cell have similar features to the SAID and PJ, but differ distinctively because of the large latitudinal extent and long durations. Different studies noted similar features without having a unique way to distinguish and categorize them. These similar features

with varying nomenclature led to confusion among scientists as a number of terms have been coined to describe the sub-auroral electric fields.

The continued use of terms such as penetration electric fields, PJs, and SAIDs could lead to misunderstanding when comparing the broad versus narrow, persistent versus transient regions of sub-auroral electric field and plasma flow (Foster 2002). Because of this, in 2002, an informal workshop assembled at the Massachusetts Institute of Technology's Haystack Observatory to discuss characteristics as well as causes and effects of sub-auroral electric fields (Foster 2002). During this time, it was agreed upon by nearly 30 experts in their respective fields that a single, well defined term was needed to describe region of electric field and sunward plasma convection in the sub-auroral ionosphere. Spatially narrow electric field structures such as the PJ and SAIDs, may or may not be apparent within such regions. The new name of SAPS was agreed upon to encompass these phenomena (Foster 2002).

Data recorded on 12 April 2001, a day with disturbed geomagnetic conditions --K_p index of 7--from the Defense Meteorological Satellite Program (DMSP) in conjunction with the Millstone Hill incoherent scatter radar is used to illustrate the SAPS occurrence. Data from this event indicate that sub-auroral plasma drifts extend from dusk across the night sector to 03 magnetic local time (MLT) and appeared at conjugate locations in both hemispheres. Both the Millstone radar and DMSP observed a SAPS event for longer than eight hours (Foster 2002) (Figure 6). The top two panels in Figure 6 show radar measurements of westward component of plasma drift and the ionospheric plasma density at an altitude of 500 kilometers. It is of note that a westward electric $\vec{E} \times \vec{B}$ plasma drift is

driven by a northward electric field in the northern hemisphere mid-latitudes. The middle panels in Figure 6 depict directional differential fluxes of down-coming auroral particles of energy ranging from 30 eV to 30 keV which delineate the auroral precipitation region (Foster and Vo 2002). The bottom panel gives the westward component of plasma velocities as measured by the DMSP flyby. The radar velocity measurements show two distinct regions of strong, broad sunward convection. The lower latitude coincides with an ionospheric density trough and a region of low overall ionospheric conductivity (Foster 2002). The vertical line in Figure 6, around 58 degrees marks the equatorward boundary of auroral electron precipitation. Westward drifts extend from this boundary to less than 45 degrees, portraying the broad extent of the SAPs. Drifts of greater than 1,000 meters per second centered around 53 degrees are collocated with the deepest plasma density trough and are characteristic of the SAID/PJ structure (Yeh 1991). The features measured near the dusk meridian of the DMSP data are displaced approximately 2 degrees poleward from the radar measurements. This shift is required to maintain current continuity across conductivity gradients near the dusk meridian (Nopper and Carovillano 1978).

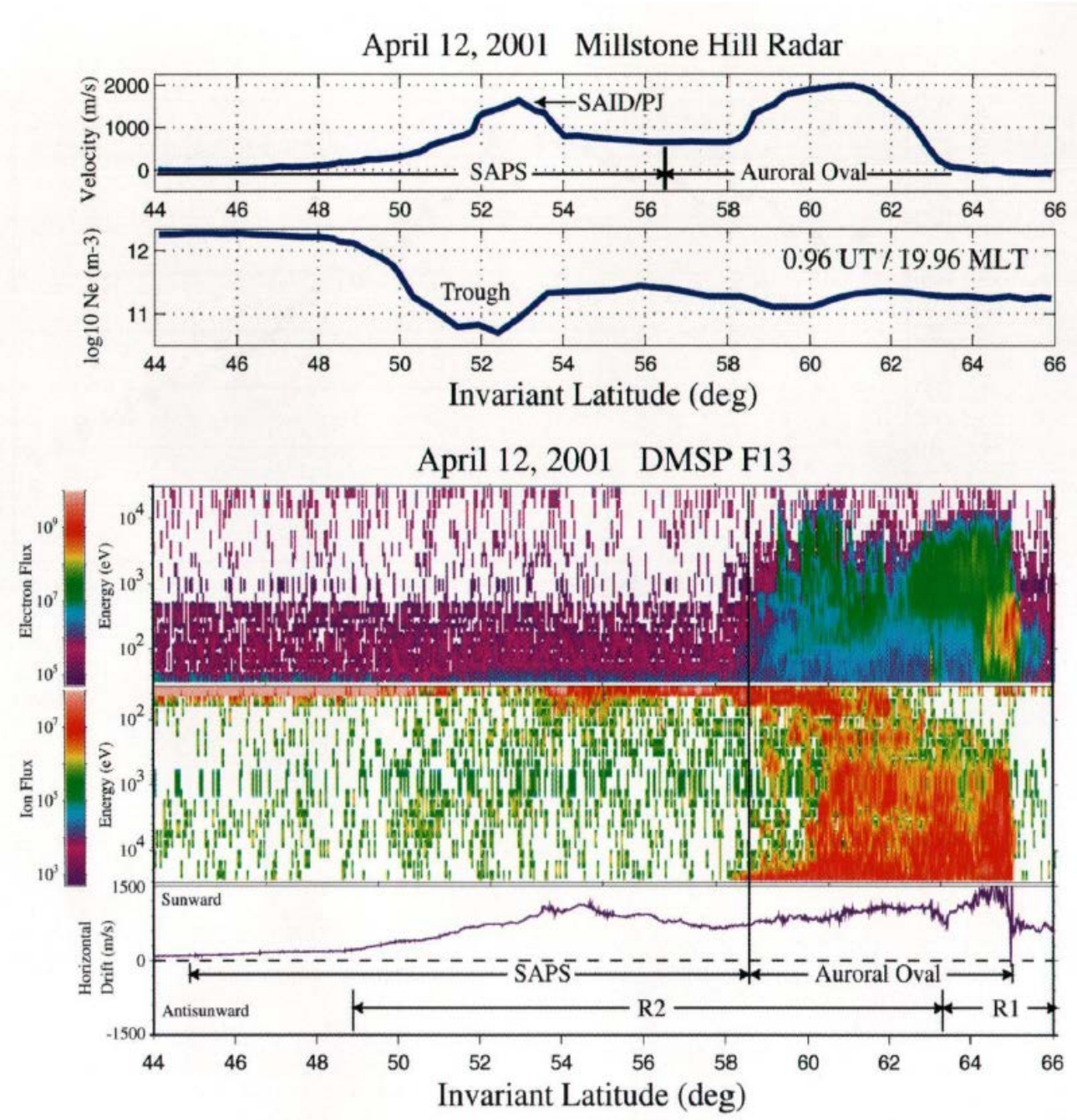

Figure 6 SAPS Data from Millstone Hill Radar (Foster 2002)

Simultaneous radar and in situ satellite measurements of auroral and SAPS plasma characteristics acquired by Millstone Hill radar and DMSP. Measurements taken at 0100Z on 12 April 2001. The SAPS is seen as a broad region of sunward plasma convection centered at 53º magnetic latitude.

SAPS are ultimately driven by the large electric potential drops enforced on the magnetosphere and polar ionospheres by the solar wind driven convection electric fields (Foster 2002). Region 1 Field-aligned currents (R1 FAC) (Figure 7) flow near the poleward border of the auroral oval, into the ionosphere on the dawn side, and out of the ionosphere on the dusk side (Iijima and Potemra 1976). To satisfy Ohm's Law, potential differences span the global ionosphere and map into the magnetosphere along magnetic field lines (Nopper and Carovillano 1978). The electric field accompanying SAPS energize ring current particles and transport them into the inner magnetosphere, which sets up a large pressure maximum on the night-side magnetosphere. Misalignments between gradients in the plasma's pressure and magnetic field volume trigger R2 FAC to flow into the ionosphere's dawn sector and out of the dusk sector (Harel 1981). A fraction of R2 FAC flow into region of low conductivity at sub-auroral latitudes. Here, large polarization electric fields are needed to maintain current continuity (Equation 5). These polarization fields generate strong plasma drifts, which create drag and heat the surrounding atmosphere by friction and enhances recombination rates, further accelerating the reduction of ionospheric conductivity (since conductivity is inversely proportional to the collision rate) within the flux tube. This acts as a positive feedback mechanism for the polarization electric field which increases and deepens the ionospheric trough even further (Foster 2002). Though these FACs may be small in magnitude, they substantially enhance the strength of the SAPS. Observed data suggested that SAPS events may continue well into the recovery phase of a geomagnetic storms after R1 FAC subside (Foster and Vo 2002). This reflects a long time required for the ring current pressure gradients to come into

alignment with the flux tube gradients. So long as these pressures are off balanced, they drive a R2 FAC that requires a large electric polarization field across deep ionospheric troughs, allowing the SAPS to persist longer than storm duration.

$$\vec{\nabla} \cdot \vec{J} = 0 \tag{5}$$

Where:

$\vec{J}$ = electric currents, A

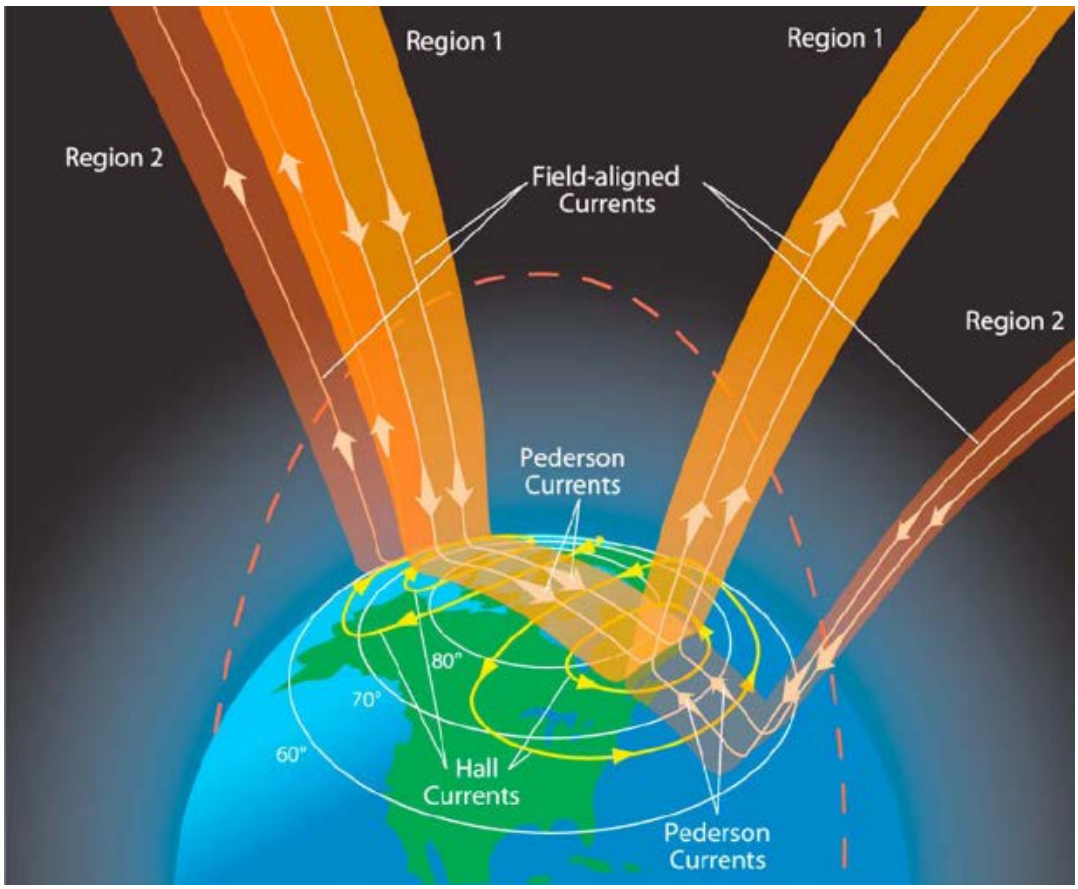

Figure 7 Field Aligned Currents & Volland Stern Pattern (Le and Slaven 2010)
Schematic of the Birkeland Field-Aligned Currents depicting the Region 1 and Region 2 currents. The R1 FAC is poleward of the auroral zone, mapping into the magnetosphere. The R2 FAC is located on the equatorward side of the auroral zone that maps down into the ionosphere auroral oval. The Volland-Stern two-cell pattern is depicted by yellow lines.

2.9 SuperDARN

Super Dual Auroral Radar Network (SuperDARN) is a collaboration of institutions in twelve countries. SuperDARN consists of 22 radars in the northern hemisphere and 11 radars in the southern hemisphere, covering the northern and southern high- and mid-latitude regions (Nagano 2015). SuperDARN operates in the HF band between 8 MHz and 22 MHz. The main goals of SuperDARN are:

1) Discover structure of global convection by providing a global scale view of the configuration of plasma convection in the high-latitude ionosphere
2) Discover dynamics of global convection by providing a global scale view of the dynamics of plasma convection in the high-latitude ionosphere
3) To test various theories of polar cap expansion and contradiction under changing Interplanetary Magnetic Field conditions and observe large-scale response of the night side convection pattern of substorms
4) Measure gravitationally induced waves in the atmosphere
5) Uncover high-latitude plasma structures and ionospheric irregularities

SuperDARN is a chain of high frequency coherent scatter radars that measure ionospheric E and F region flow velocities in the line-of-sight directions. SuperDARN utilizes an array of electronically phased antennae that can be steered to look in 16 or more beam directions stepping in azimuth every 3.3 degrees with temporal resolution of one to two minutes (Greenwald et al., 1995). Beams are numbered sequentially starting with 0 for the most westward looking beam. For each direction, the radar detects backscatter echoes beginning at 180 km and extends to a maximum range of about 3500 km. Figure 8 illustrates how the SuperDARN system scans the ionosphere.

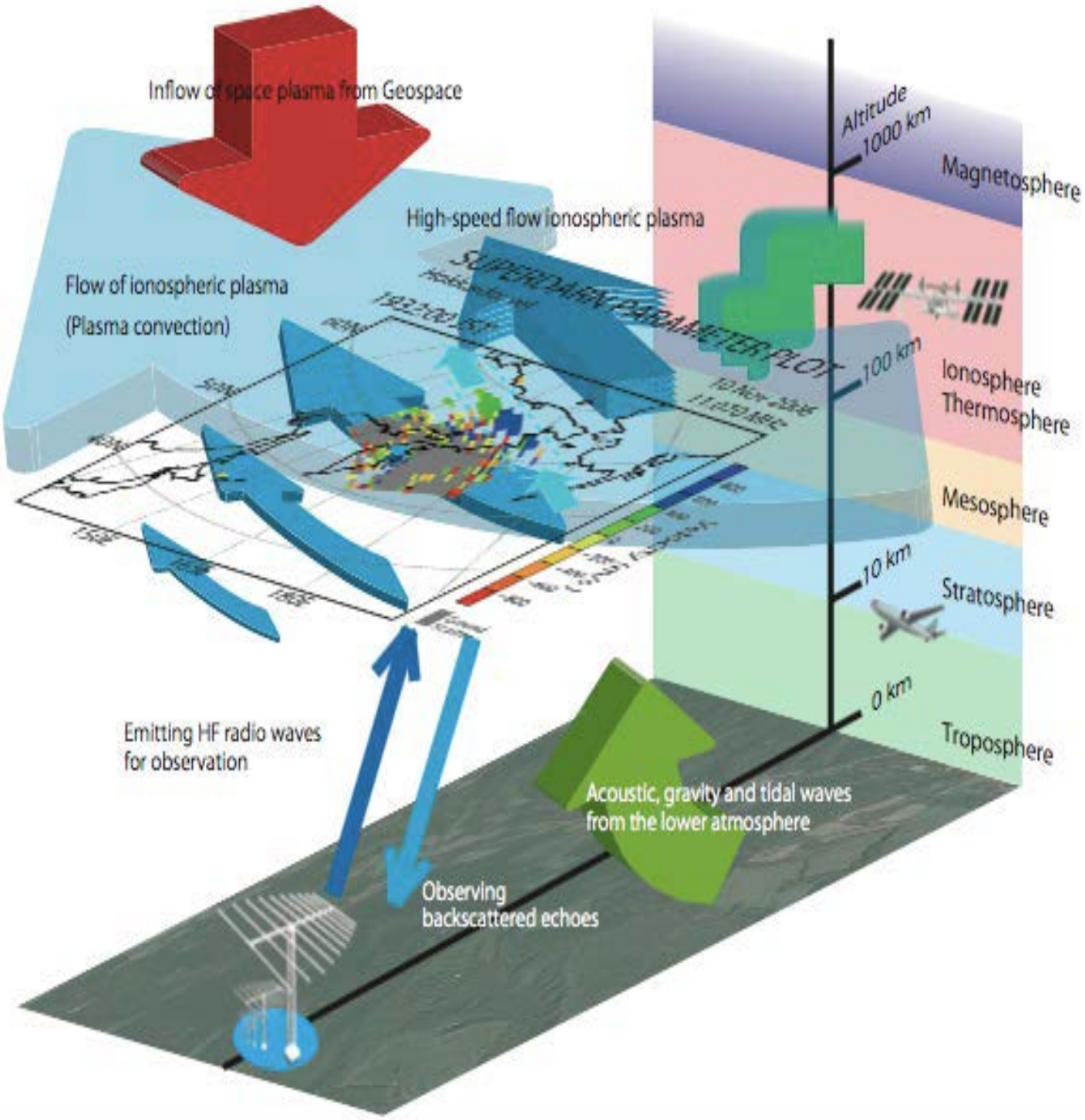

Figure 8 Flow of SuperDARN Ionosphere Scanning (Nagano 2015)

Flow of data collection from SuperDARN. Illustrates how network monitors ionospheric parameters to localize anomalies and collects data to be assimilated into ionospheric models.

Figure 9 illustrates the SuperDARN radar coverage of the geographic North Pole. The radar stations used in this study are located in Saskatoon (SAS), Prince George (PGR), King Salmon (KSR), Fort Hays East (FHE), Fort Hays West (FHW), Christmas Valley East (CVE) and Christmas Valley West (CVW). The FHE and FHW radars were available from November 2009, and the CVE and CVW radars were available since the middle of January 2011.

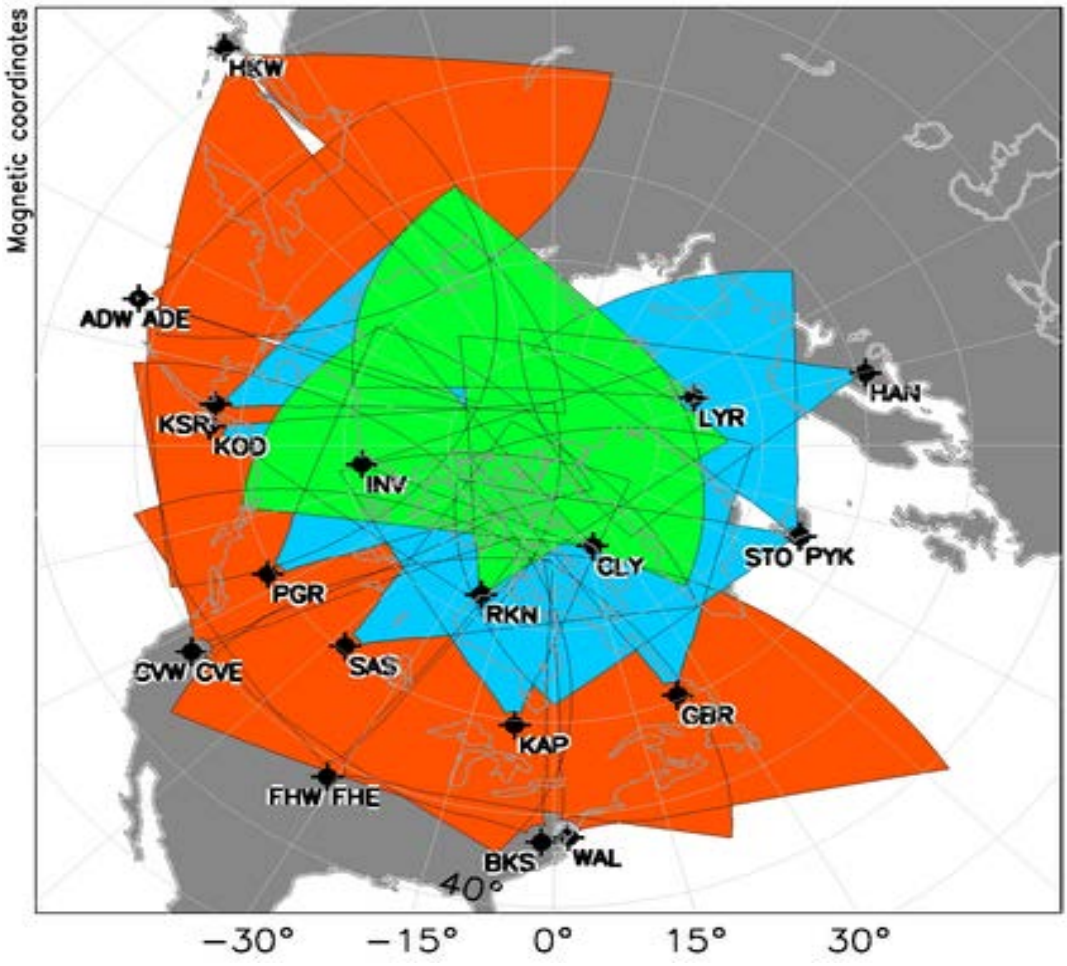

Figure 9 SuperDARN Coverage Map (Virginia Tech)

SuperDARN Radar coverage along the North Pole. Green depicts coverage along the polar cap while blue shows the high-latitude coverage. The orange represents mid-latitude coverage.

2.10 OVATION Prime

The OVATION Prime model was developed using energetic particle measurements from the polar-orbiting Defense Meteorological Satellite Program (DMSP) satellites and considers four types of aurorae: two types of discrete electron aurorae (1A: mono-energetic and 1B: broadband) and two types of diffuse aurorae (2A: electron and 2B: ion) (Newell et al., 2010). The OVATION Prime model is written in Interactive Data Language (IDL) and was developed at Johns Hopkins Applied Physics Laboratory by Patrick Newell. The model provides a statistical distribution of auroral precipitation in the ionosphere obtained from 11 years of DMSP electrostatic analyzer data. Observations have been binned by magnetic local time and latitude and by solar wind parameters (solar wind velocity, interplanetary magnetic field components, and electron density) as measured by the Advanced Composition Explorer (ACE) satellite prior to 2016 and then Deep Space Climate Observatory (DSCOVR) spacecraft after 2016.

In order to test the reliability and accuracy researchers evaluated the ability of the OVATION Prime auroral precipitation model to provide operational forecasts of the visible aurora. Nighttime model forecasts were validated with Polar Ultraviolet Imager data for K_P greater than or equal to 3 during 1997 and 1998. The overall forecasts for a visible aurora to occur or to not occur were correct 77% of the time. The most important prediction for public auroral viewing is that the visible aurora will occur, and these forecasts were correct 86% of the time (Machol 2012). Similarly, a study was conducted comparing the statistical analysis of all auroral models. Each model's energy flux output was compared to DMSP data in a variety of categories including: high, moderate, and low Kp index

conditions; dawn, day, and dusk magnetic local time (MLT) sectors; and all four seasons (Lane 2012). Lane (2012) discovered that the OVATION Prime model outperformed eight other models in six categories and was the model with the highest overall prediction efficiency score. OVATION Prime was deemed to be the most accurate of the models and most suitable for operational auroral forecasting. While OVATION Prime is the preferred model for auroral forecasting, there is no previous literature that examines the model's performances equatorward of the auroral oval. One intent of this study is to push the operational limits of OVATION Prime to see if its operational range can be extended into the sub-auroral latitudes to act as a proxy for mid-latitude modeling.

OVATION Prime uses a color coded output for particle energy flux that ranges from 0 up to 8 $ergs/cm^2s$. These units are equivalent to milliwatts per square meter in SI units (Newell 2010). The energy flux output has 20 colored pixels that covers the 8 $ergs/cm^2s$ range of the model's output (Figure 10). This yields a resolution of 0.4 $ergs/cm^2s$ per colored pixel.

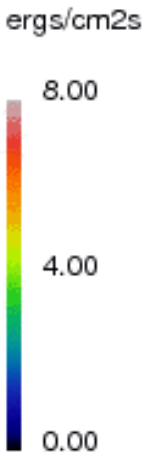

Figure 10 OVATION Prime Output Color Scale (CCMC)
Particle energy flux output display values from the OVATION Prime model.

2.11 Summary

SAPS are classified by rapid westward (sunward) plasma flows located equatorward of the auroral oval and predominantly in the dusk and pre-midnight sectors (1600-2400 MLT). They can change the ionospheric composition, lead to storm-enhanced density and plasmaspheric plumes, produce very large field aligned vertical flows, and form the F region density troughs. When the Kp index is greater than 4, the SAPS in the pre-midnight sector form at 60 degrees magnetic latitude, span 3-5 degrees in latitude, and have an average peak amplitude of more than 900 meters per second. The occurrences of SAPS are associated with sub-storms and storms. SAPS has varying levels of intensity and spatial extent and is seen as a persistent feature of the disturbed night-side convection pattern. The position, extent, and intensity varies with changing solar activity. The most probable local time of SAPS is found to be during 2100 and 2300 MLT, with most pronounced features happening around 2200 MLT. Foster and Vo (2002) report the magnetic latitudes of SAPS are linearly related to the magnitude of Kp index, meaning the higher the Kp index the further equatorward the latitude of SAPS events. The location of SAPS is conjugate to the peak ring current energy density and the R2 FACs, and coincides with the equatorward edge of the ion plasma sheet. SAPS spans the lower ionosphere conductivity region between the equatorward edge of plasma sheet particle precipitation and the plasmapause (Foster 2002). The SAPS location is the consequence geomagnetic storming, and is dependent on the Kp index.

An extensive literary search shows no previous research has made an attempt to predict the occurrence of SAPS, nor has an attempt been made to find a correlation to a

physical parameter that could add insight as to when and where the SAPS occur. Foster and Vo (2002) found a correlation of occurrence tied to the Kp index, but that does not provide insight into the location of the SAPS stream. Currently, the primary way to discover and locate SAPS is by using real-time ionospheric sampling radars or the Defense Meteorological Satellite Program (DMSP) to find the rapid westward flow. After the ionosphere is sampled, space weather technicians must then analyze the data to discover the SAPS. The objective is to establish an operational threshold "quick-look" parameter to identify the occurrence of SAPS without having to monitor real time ionospheric radar data.

3 Methodology

3.1 Chapter Overview

This chapter will discuss the tools needed for obtaining accurate data on SAPS and correlating them to particle energies outputted from OP. The methodology will explain the specific threshold criteria to classify a SAPS events as well as how SAPS characteristics and parameters are calculated. Next explained is how OVATION Prime is used to determine the particle energy flux values. Finally, the process by which the data is examined will be outlined.

3.2 SAPS Occurrence Identification

Similar to Foster and Vo [2002] a standard set of criteria will be used in identifying the sub-auroral polarization stream convection velocity region in the radar scan data. For this study, SAPS will be defined as a clearly identifiable region of westward convection velocity equatorward of the low-latitude edge of the auroral zone. There is an element of subjectivity in this application but the method gives repeatable, consistent results. SuperDARN radar returns will be used to identify SAPS occurrences. Baker et al (2007) determined this methodology to be effective in determining ionospheric convection and plasma flow. Figure 12 is a scan of a SuperDARN radar showing the radar capturing the SAPS event. The aurora is poleward of 62 degrees magnetic latitude as indicated by the dashed line. Slightly equatorward of the aurora the flow towards the radar was more than 500 m/s. At the same time DMSP F15, represented by the black bar graph lines going from lower left to upper right, observed strong westward flows.

3.3 Parameter Calculations

Most parameters required in this thesis such as dates, times, elevation angle, and geomagnetic coordinates are simply documented from radar scan information. SAPS maximum westward flow is calculated, not directly measured. Radar time stamps and ray tracing tools are used to gauge velocity. Ray tracing tool allows users to select and follow the flow of a specific radar return. The distance is based upon how far the return has moved from the previous scan. Next, time stamps from the radar output image are used to determine time taken to travel distance from ray tracing. From the combination of these data points, a velocity is calculated to determine western flow speed. Figure 9 clearly portrays that no two radars have the same azimuthal coverage angle, nor do any point perfectly north- south or east- west. This creates a combination of east-west and north-south components of each beam line-of-sight. In order to correct for this, the beam viewing angle is taken from radar scan information, converted into radians, and a simple geometry adjustment finds the maximum magnitude of western SAPS flow. Max flow is calculated by using raw western flow determined by successive radar scans and ray tracing, which is corrected by dividing the cosine of the beam angle (in radians) ensuring all calculated velocities capture only the westward flow which is a flagship signature of SAPS. Figure 11 illustrates this correction process.

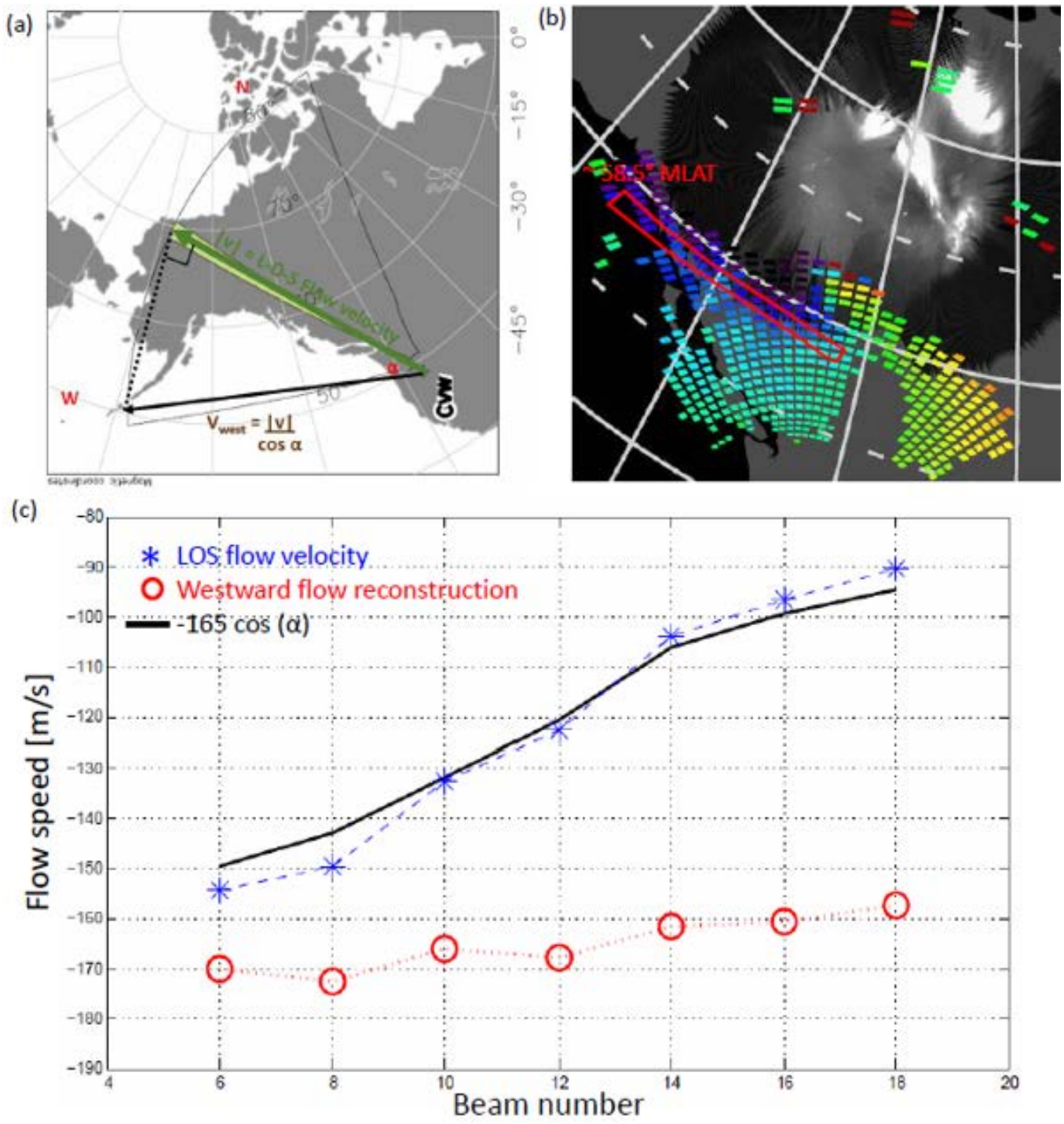

Figure 11 Westward Flow Reconstruction

Panel (a) shows the geometry of a westward looking radar, panel (b) is the raw radar flow data, and panel (c) shows the westward flow reconstruction based upon the geometry. The negative signs represent the direction of flow (westward).

3.4 OVATION Prime Synchronicity (Simultaneity)

A key piece of this study is not only identifying SAPS occurrences, but also being able to collocate these events, both spatially and temporally, within a separate model with differing resolution scales. Conveniently, SuperDARN radar scans and OVATION Prime model output use similar graphic user interface and plot spatial information in magnetic coordinates. No location correction is required to go from one to the other. The temporal resolution is no different. Information from SuperDARN scans and OVATION Prime particle energy flux values are available in five-minute increments starting on the hour. When the westward plasma flow associated with a SAPS event begins the specific time is recorded. The time of identified maximum plasma flow is logged as well as when SAPS flow decreases below the initial background value. These times signify the start, time of max flow and end time of SAPS events. This process is not intended to capture the exact moment a SAPS event starts, but rather to comprehend if SAPS streamers are detectable in modelled energy flux output. In order to maximize the probability of detection, the time of max westward flow is used, rounded to the nearest five-minute increment. After the time is identified, it is a simple evaluation on OVATION Prime; find the magnetic coordinates of the SAPS streamer and record the particle energy flux observed. Figure 12 outlines identified SAPS flow on radar while Figure 13 captures the OVATION Prime total particle energy flux from the same event identified in Figure 12.

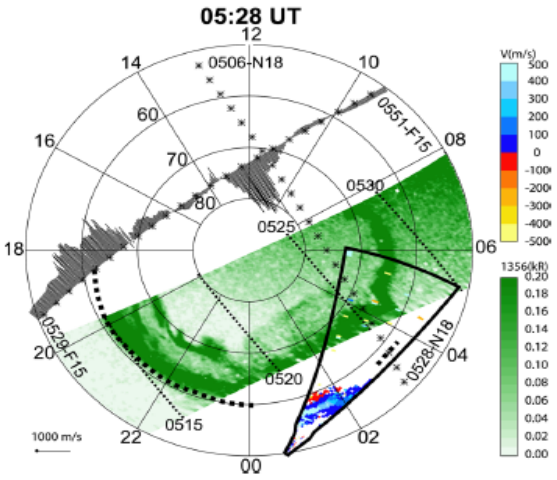

Figure 12 SAPS Flow Captured on SuperDARN

SuperDARN scan from Wallops radar displayed versus magnetic latitude and magnetic local time. The radar's line of sight is indicated by the solid black triangular swath. The green scale is the aurora data obtained from DMSP and NOAA-18 satellites. The thick dashed lines indicate the auroral boundary. The black bar graph line shows the path and measurements of the DMSP F15 spacecraft. Bars above the line show eastward flow, while the lines below indicate westward flow.

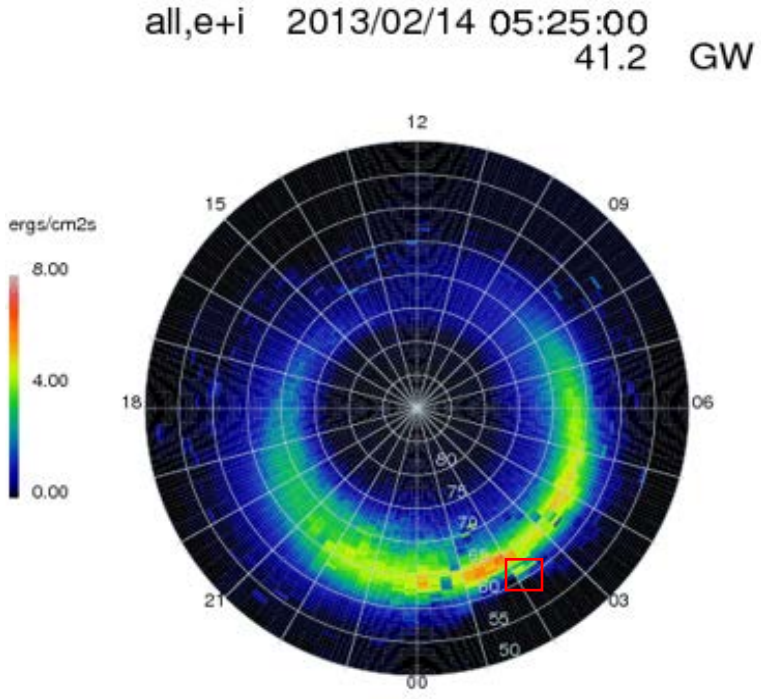

Figure 13 OVATION Prime Energy Flux during SAPS Event (CCMC)

OVATION Prime all particle energy flux corresponding to same SAPS occurrence from Figure 12, outlined in red. The SAPS stream is seen just equatorward of the auroral boundary. In this case, the SAPS stream is associated with a total particle energy flux of 4.4 ergs/cm^{2}s.

3.5 Data Analysis Process

Information on SAPS and energy fluxes during events establish an extensive dataset. The process by which the data is displayed is a scatter plot. It is the intent to use OVATION Prime output as a proxy for real-time ionospheric measurements. Because of that, the particle energy flux is set as the independent variable (x-axis) while the maximum western flow of SAPS is plotted as a function of particle energy (y-axis). Once plotted, a line-of-best-fit connects the data points and the trendline that displays the highest regression value is the one that is used, ignoring any polynomials higher than second order. Next, histograms are used to reveal the common traits within the dataset. The histograms are then used to create pie charts to show each piece compared to the whole.

3.6 Summary

Once a SAPS event has been identified, the occurrence, closest to the model's time and spatial resolution, is evaluated on the OVATION Prime model to determine what energy fluctuations are associated within the SAPS stream. The data is then analyzed both by common occurrence as well as a function of SAPS flow speed to uncover any relationship that exists. Finally, the correlations are used to create forecasting methods in order to use existing architecture to predict clutter and signal fading impacts to HF operations.

4 Analysis

4.1 Chapter Overview

In this section the data will be examined in order to look for a connection between particle energy flux and SAPS occurrences. A database of energy flux of all SAPS events will be plotted to see which energy flux best captures the SAPS streams. Next, the velocity of westward plasma flow within the SAPS stream will be analyzed against both electron energy flux and total particle energy flux to determine if particle energy flux plays an important part in the flow velocity of SAPS streams. As the data reveals the relationship, the information will be used to develop operational methods to determine the feasibility of using particle energy flux as a tool to forecast SAPS events.

4.2 Data Analysis

First, after compiling detailed information of 87 SAPS occasions, a histogram of particle energy flux is created in order to discover the most common flux values associated with SAPS events (Figure 14). Data reveals that for electron energy flux there are two values that hold the plurality, 3.6 and 4.4 ergs/cm^2s. These flux values are observed 16.9 percent of the time. The second most common electron flux value is 4.0 ergs/cm^2s occurring in 10.3 percent of identified events. A full break down of each electron flux values from OVATION Prime is illustrated in Figure 15. Next examined is the commonality of total particle energy flux values, both ions and electrons. Figure 16 is a histogram of OVATION Prime's total particle energy flux output. In this instance, there is only one value that occurs most often, 4.0 ergs/cm^2s, which materializes in 16.1 percent

of the time. There are two values for the second most common total particle energy flux values, 3.6 and 4.4 ergs/cm^{2}s. The latter two values also coincide with the most common electron energy flux values, making them the prevailing flux values during SAPS events. The flux values of 3.6 ergs/cm^{2}s and 4.4 ergs/cm^{2}s are each observed in 25 of 87 SAPS events, showing up 28.7 percent of the time, while cumulatively occurring in 50 out of 87 SAPS events, resulting in these energy flux values being modelled 57.5 percent of all SAPS streamer occurrences. While 3.6 ergs/cm^{2}s and 4.4 ergs/cm^{2}s are the most reoccurring values, the average value across all particle energy flux is 4.0 ergs/cm^{2}s.

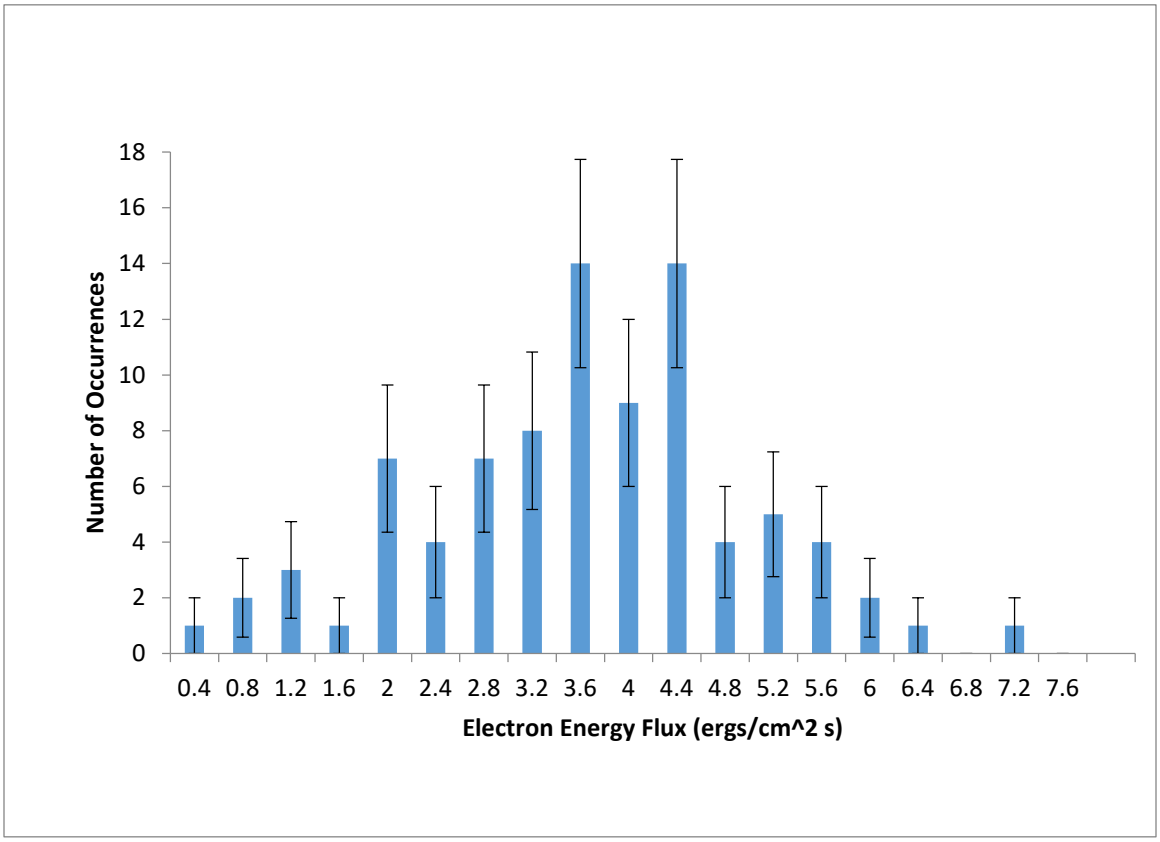

Figure 14 Electron Energy Flux Histogram
Histogram of electron energy flux occurrences during identified SAPS events with associated Poisson Counting error bars related to the square root of the count.

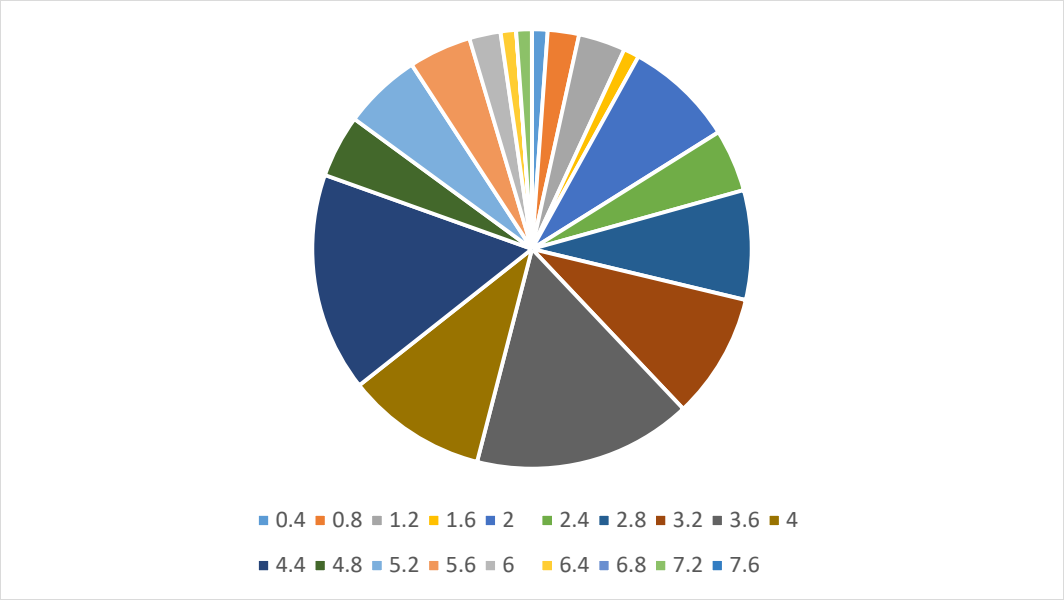

Figure 15 Electron Energy Flux Pie Chart

Percentage occurrence of each electron energy flux output value from OVATION Prime. 3.6 and 4.4 ergs/cm^{2}s were both the most common values, happening 16.1% of the time.

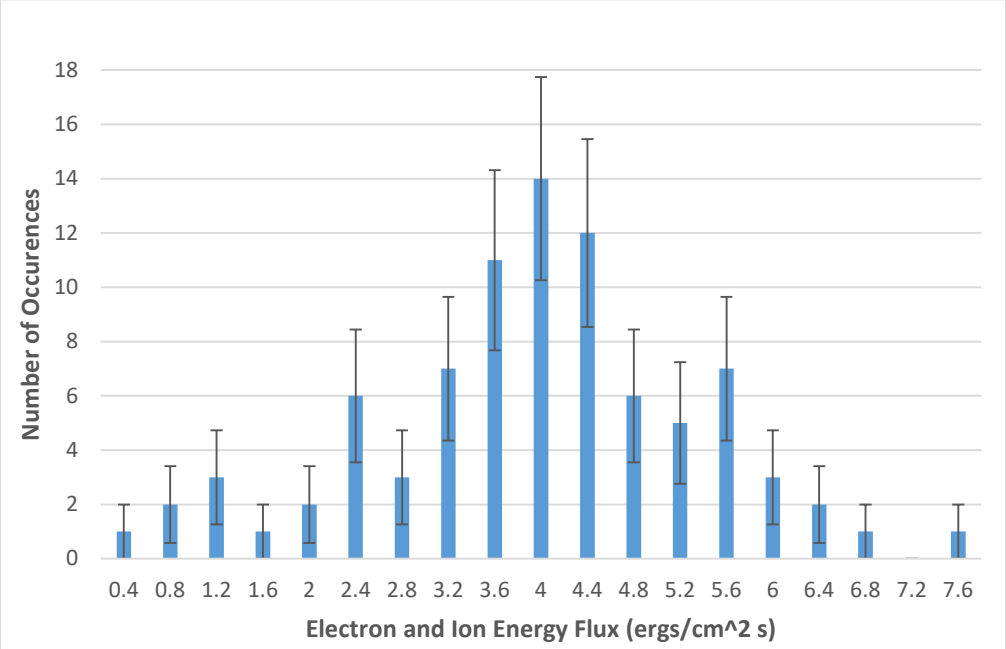

Figure 16 Histogram of Total Particle Energy Flux

Histogram of total particle (electrons and ions) energy flux occurrences during identified SAPS events with associated Poisson Counting error bars related to the square root of the count.

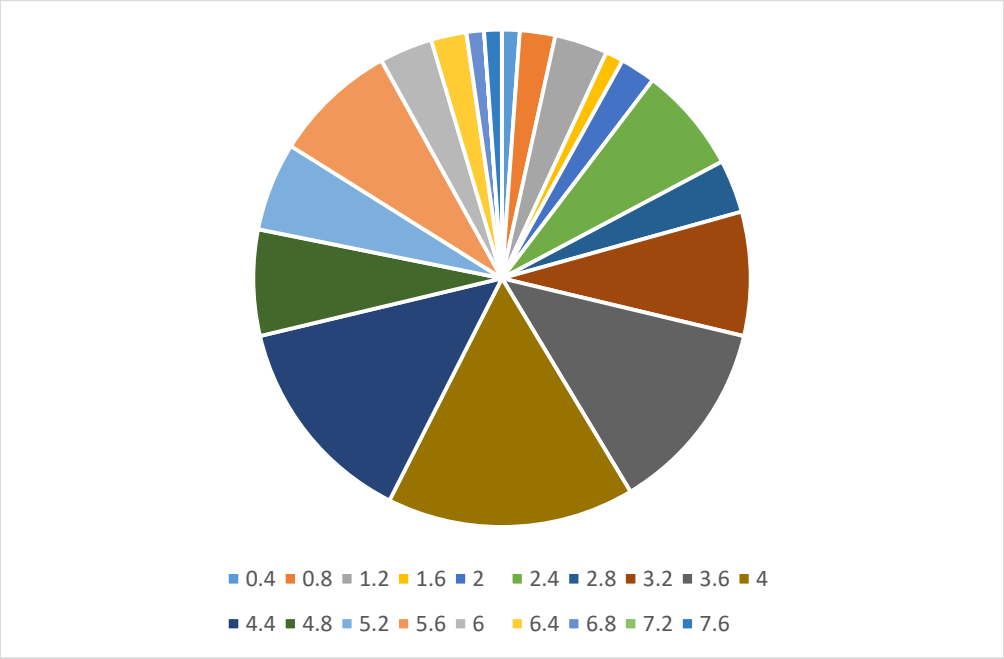

Figure 17 Total Particle Energy Flux Pie Chart

Percentage occurrence of each total particle (electrons and ions) energy flux output value (ergs/cm^{2}s) from OVATION Prime. 4.0 ergs/cm^{2}s was the most common value, happening 16.1% of the time.

Previously, the specific energy flux values were simply accounted for during all SAPS events to identify the most occurring output value. Next examined is the SAPS maximum flow velocity in an attempt to uncover if the particle's energy flux value plays a role in impacting the velocity of the SAPS streamer. Figure 18 shows the maximum magnitude of SAPS plasma drift values as a function of modelled electron energy flux values. Interestingly, the line-of-best-fit is an exponential decaying function described by $1940\ e^{-0.292x}$ with an R squared value of 0.582. Linear, logarithmic, quadratic polynomial and power trends were also examined, but the exponential had by far the best R squared value. This trendline suggests that the faster plasma drift values are associated

with lower particle energy flux values while the slower flow occurs when OVATION Prime models higher electron energy flux outputs.

Figure 19 is a scatter plot, again using the maximum magnitude of SAPS flow velocity but this time as a function of total particle—both ions and electrons—energy flux values. Once more, the best fit trendline reveals an exponentially decaying relationship between the two. The equation for the trendline is given by $1985.5\, e^{-0.275x}$, similar to using electron energy flux, however with a lower R squared value of 0.522 and a slightly smaller decay constant (-0.275 compared to -0.292). Both total particle energy flux and electron energy flux seem to be telling the same story of an inverse relationship between particle energy and maximum SAPS flow speeds.

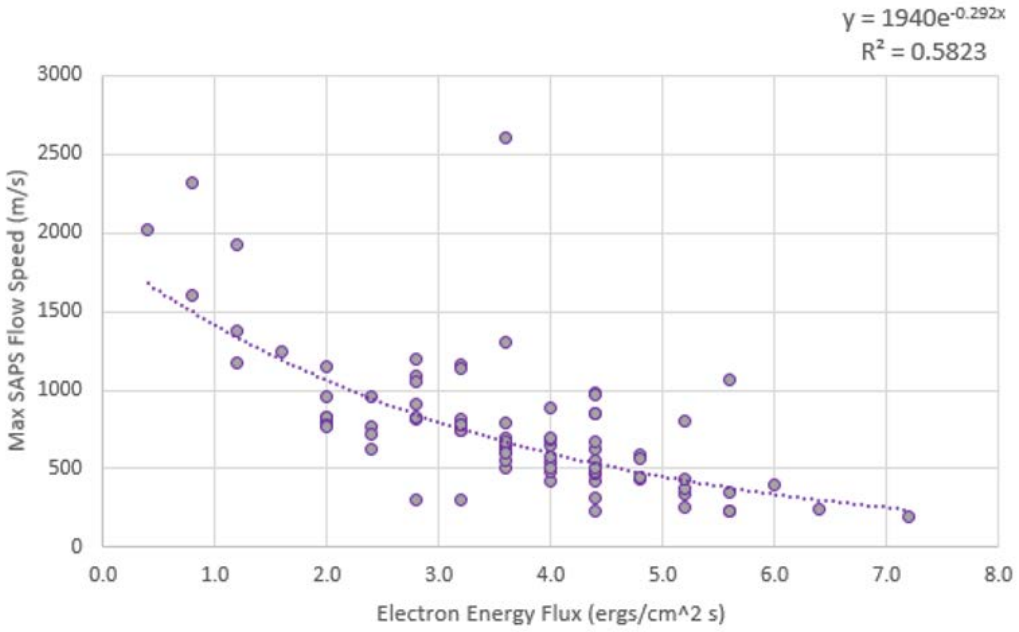

Figure 18 SAPS Flow Speed versus Electron Energy Flux

Scatter plot of maximum SAPS flow velocity versus electrons energy flux. Graph shows a slight exponentially decaying relationship. The faster the SAPS velocities are associated with lower electron energy flux whereas the slower SAPS velocities are associated with higher electron energy flux values.

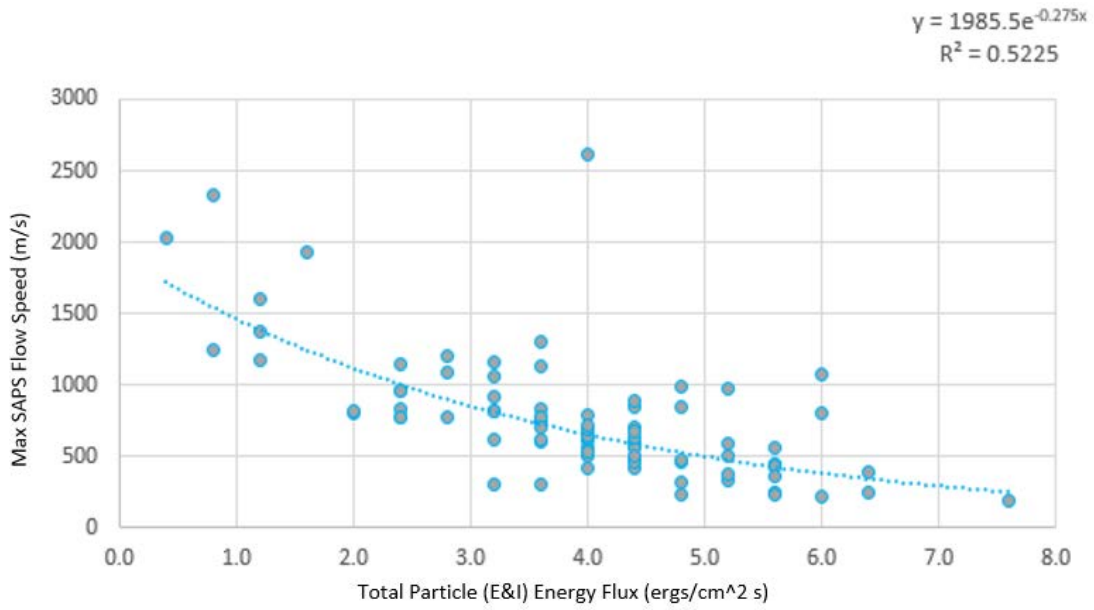

Figure 19 SAPS Flow Speed versus Total Particle Energy Flux

Scatter plot of maximum SAPS flow velocity versus total particle (electrons and ions) energy flux. Graph shows a slight exponentially decaying relationship. The faster the SAPS velocities are associated with lower total particle energy flux whereas the slower SAPS velocities are associated with higher total particle energy flux values.

While compiling information on SAPS events and energy flux relations, a separate pattern began to reveal itself—the time of year in which SAPS occurred. Out of the 87 cases identified, 73 identified events occurred during the months spanning from January to May. 83.9 percent of SAPS streamers occurred in the first half of the year, while only 14 (16.1 percent) happened in the later half. Figure 20 is a histogram showing the number of SAPS events broken down by month. This reveals a strong seasonal dependence with a distinct predilection of occurrences happening after the autumnal equinox but before the vernal equinox (October through March) with 61 SAPS events (70.1 percent) identified during this timeframe. Figure 21 shows the comparative percentage of identified SAPS by

month. March contained the most SAPS events with 25 (28.7 percent) while June, August, and November tied for the least amount at one event in each month (1.1 percent each).

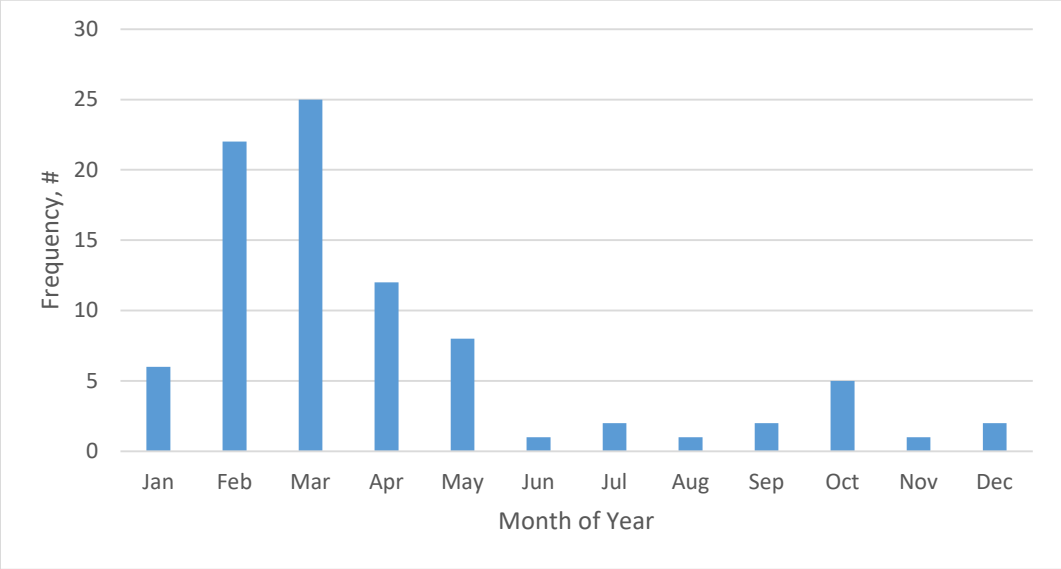

Figure 20 Monthly Frequency of SAPS
Bar graph showing how many SAPS streamers were identified in each month of the year.

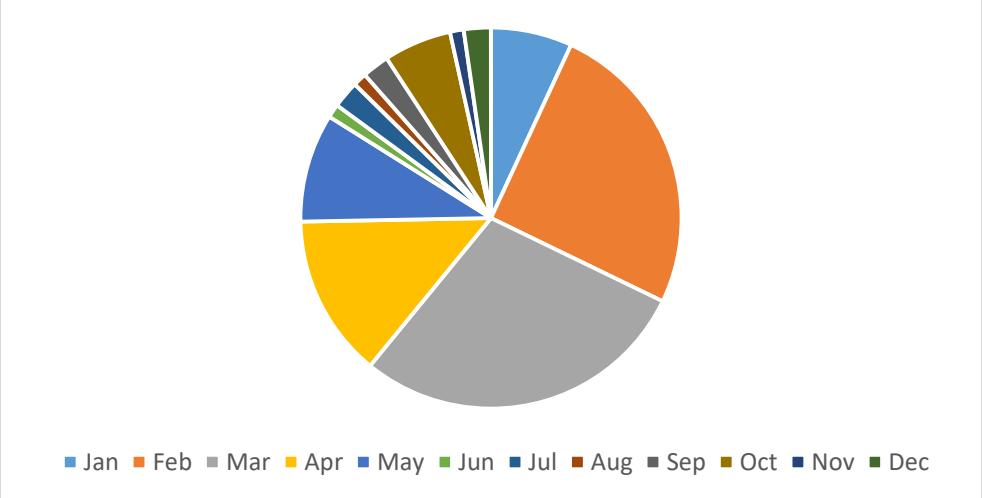

Figure 21 SAPS Frequency Percentage by Month
Pie Chart depicting percentage of SAPS occurrences broken down by month

Next, the data is cataloged into SAPS streamers found during solar minimum and those found during solar maximum. In this instance, solar minimum is defined to be the concluding portion of Solar Cycle 23 which encapsulates data from December 2007 through April 2010, while solar maximum is taken to be the upswing in Solar Cycle 24 which captures data from October 2010 through April 2013—of note, there is a natural break in the data as no events were identified between April 2010 and October 2010. Similar to the process as before, the maximum speed values are plotted as a function of particle energy flux. First examined is the relationship between maximum plasma drift speed and electron energy flux values during solar minimum, as shown in Figure 22. The relationship is best described by an exponentially decaying trendline, governed by the equation $1167\mathbf{e^{-0.225x}}$. This time, however, the $\mathbf{R^2}$ value climbs to 0.658. Second examined is the correlation of max speed to ion and electron energy flux during solar maximum, shown in Figure 23. Comparable to previously examined correlations, the line of best fit is an exponential decay given by the formula $1652\mathbf{e^{-0.194x}}$ with a lower $\mathbf{R^2}$ value of 0.485. The plots are recreated using total particle flux values compiled by solar minimum and solar maximum. Figure 24 is a scatter plot of max flow speed versus total particle flux values during solar minimum. Again, an exponential decay function given by $1197\mathbf{e^{-0.214x}}$ best describes the plotted data, however having an $\mathbf{R^2}$ value of 0.333 it is the worst fit seen yet. Figure 25 shows the data of maximum SAPS flow speeds as a function of total particle energy flux during solar maximum. For the first time the trendline is not an exponential but rather a power function. The line-of-best-fit equation is $1486\mathbf{x^{-0.451}}$ with an $\mathbf{R^2}$ value of 0.476 whereas the exponential trendline has an $\mathbf{R^2}$ value of 0.381.

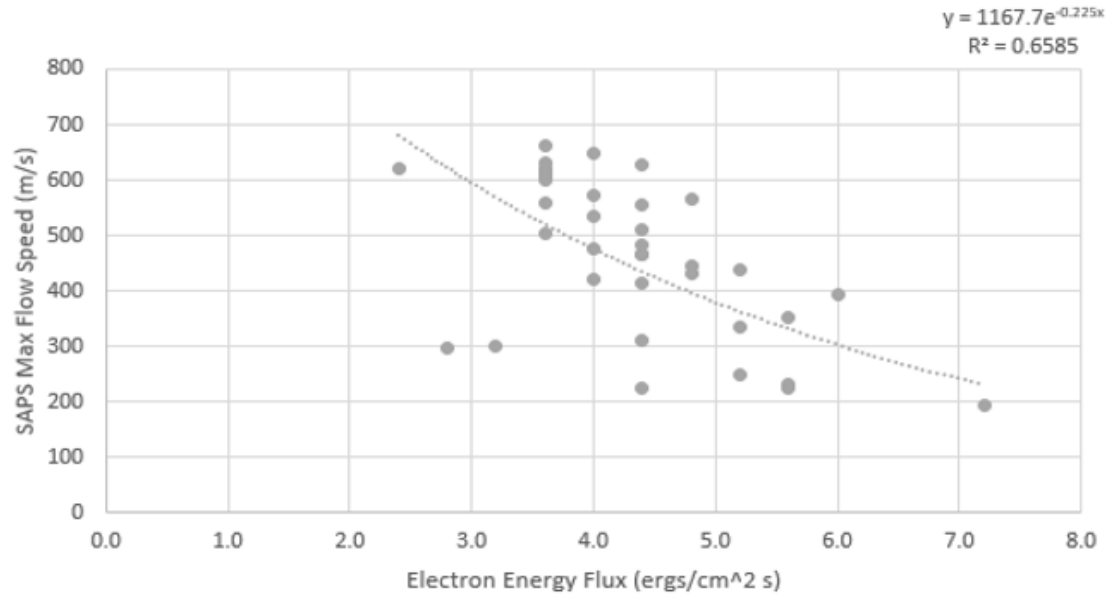

Figure 22 Max SAPS Flow Speed vs Electron Energy Flux: Solar Minimum

Scatter plot of maximum SAPS flow velocity versus electrons energy flux. Same as Figure 18 with data filtered for solar minimum. Again graph shows a slight exponentially decaying relationship, but this time with a higher R^2 value.

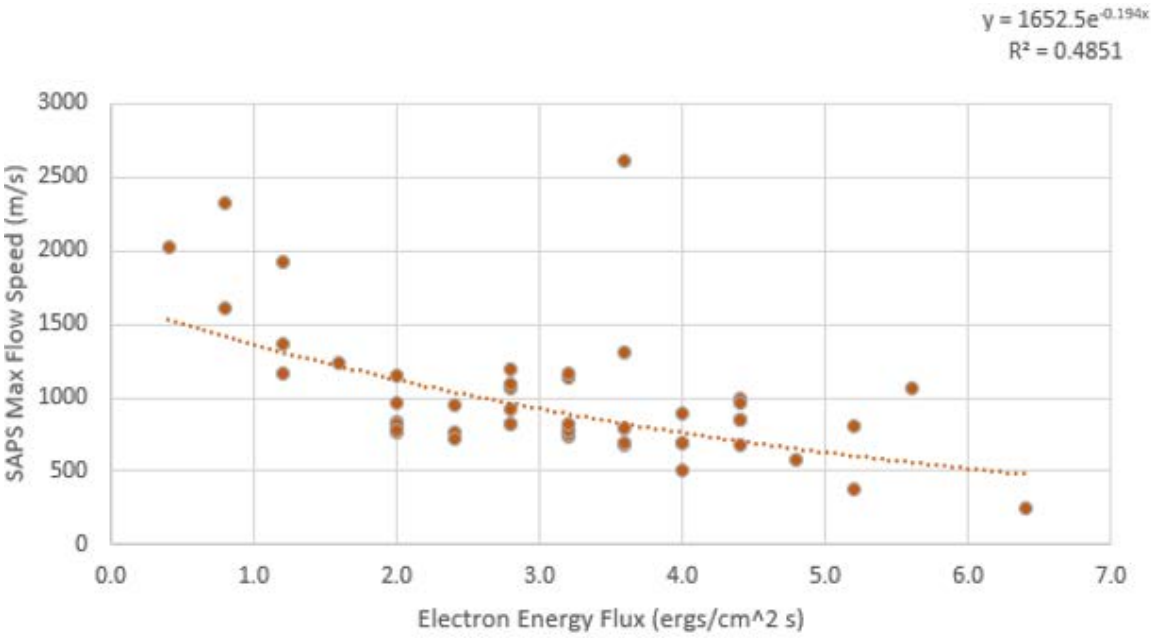

Figure 23 Max SAPS Flow Speed vs Electron Energy Flux: Solar Maximum

Scatter plot of maximum SAPS flow velocity versus electrons energy flux. Data is filtered to only show events during solar maximum. Relation still best described by exponential decay, however with a lower R^2 value

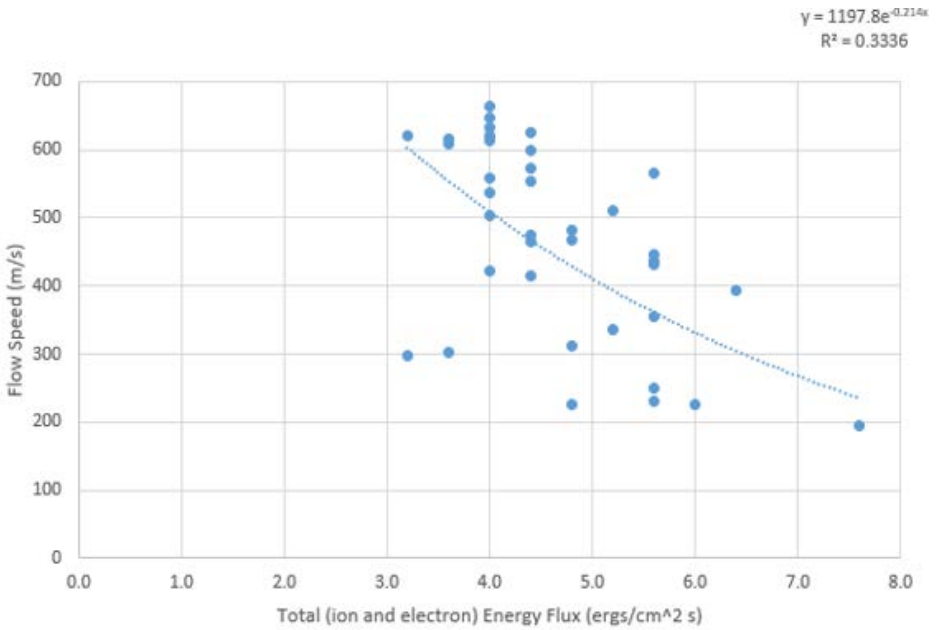

Figure 24 Max SAPS Flow Speed vs Total Particle Energy Flux: Solar Minimum

Scatter plot of maximum SAPS flow velocity versus total particle energy flux. Data is filtered to only show events during solar minimum. Data still exhibits exponential decay correlation, however with a much lower R^2 value than previously seen from Figure 18

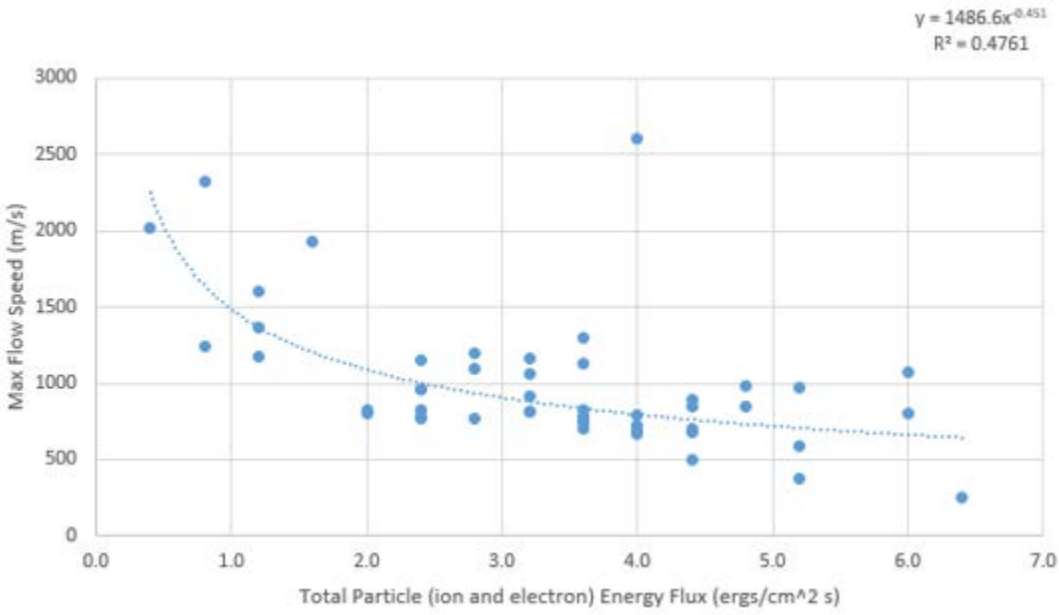

Figure 25 Max SAPS Flow Speed vs Total Particle Energy Flux: Solar Maximum

Scatter plot of maximum SAPS flow velocity versus total particle energy flux. Data is filtered to only show events during solar maximum. Unlike total event data in Figure 19, solar max data is best fit by power series, nearly $1/\sqrt{x}$, though the R^2 is lower by 0.046

4.3 Conclusion of Research

Data analysis of particle energy flux versus maximum magnitude of SAPS flow velocities reveals a slight connection of SAPS maximum flow magnitude to modelled particle energy flux, most of which are an exponentially decaying relation best described by $e^{-0.240x\pm0.037}$. The decay coefficient (-0.240) is determined by the calculated mean of all plots best described by an exponential trendline while the error (± 0.037)is one standard deviation from the same data. The exception to the exponential relationship is total particle energy flux during solar maximum. This relationship is best represented by a power law fit proportional to $x^{-0.451}$. Since there is only one data point for the power fit, no error is calculated. Scrutinizing the scatter plots reveals some outliers that may be contaminating the data, skewing the trendlines. This is evidenced by the mean R-squared value of 0.516 ± 0.109 found by calculating all plots of SAPS velocity versus particle energy flux to include electron, total particle, electron during solar min, electron during solar max, and total particle flux during solar min. This modest R-squared value indicates only moderate confidence in the exponential decay function's ability to represent the data. Other factors that may play into the lower R-squared value is the binning of OVATION Prime having limited output values, as well as the data being a multi-valued function. Sectioning the analysis into two parts, solar min and solar max, helps alleviate these outliners and improves trendline fits when examining just electron energy flux values, however the multi-valued function problem persists. During solar minimum, the R^2 value increased from 0.5823 in Figure 18, to 0.6585 in Figure 22. In fact, this is the best-fit correlation (R^2 value) suggesting electron energy flux is the best parameter to identify SAPS flow on

OVATION Prime. Conversely, the R^2 value dropped to 0.4851 when electron energy flux is sectioned out into solar maximum. When investigating total particle energy flux, the R^2 value decreased for both solar minimum and solar maximum. During solar minimum, the R^2 value for total particle flux plummeted to 0.3336, the worst fit of any plot. For solar maximum, the line of best bit switched to a power law representation. While the R^2 value decreased to 0.4761, it is still an improved fit over the exponential during that timeframe which had an R^2 value of 0.3709.

Within Figure 18 and Figure 19, a tighter grouping exists between energy flux values of 2.0 and 6.0 ergs/cm^2s as well as SAPS flow velocities below 1600 meters per second. This section of the scatter plots advocate the correlation is best used during moderate geomagnetic storming conditions and best captures the routine SAPS streamer and does not handle the extremes very well. The fit function moderately represent the slower limit of SAPS velocities but inadequately captures the faster limit of SAPS velocities, which explains why the R^2 value decreased for electron energy flux during solar maximum. From this, it appears that there is a correlation between energy fluctuation and the fastest SAPS speeds, although it does not appear to be a direct correlation. One cannot look independently at modelled electron energy flux to surmise SAPS flow speeds, nor does it follow an empirical equation. Operationally, it must be used as a tool in conjunction with other data.

Splitting the collated SAPS data into temporal bins reveals that late winter/early spring (Feb-Mar) is when SAPS events are most likely to occur. There is a definite symmetry about the equinoxes with localized seasonal peaks in March and October. It is

conjectured that the polar cap potential, which is highest near the equinoxes (Kelley 2009), plays an important role. If this truly is the case, then why not have a similar number of instances during the autumnal equinox (i.e. 25 in March versus only 5 in October)? The data in this thesis is taken from the Northern Hemisphere. It is conjectured that the during the winter months when the pole is in total darkness, the atmospheric conductivity drops, which is known to be an important factor in driving SAPS formation. It would be intriguing to view SAPS data from the Southern Hemisphere to see if there is a predominant peak in September/October (Southern Hemisphere vernal equinox) versus February/March (Autumnal equinox) to test this theory. At this point, it is still unclear why this vernal preference occurs and will be a topic for future research.

Another commonality suggests a separate correlation exists between particle energy fluxes and observed SAPS events. Combining information from plotted histograms of electron (Figure 14) and total particle energy flux (Figure 16) reveals that 51 of 87 (58.6 percent) of SAPS events in this study have an energy flux value of either 3.6 ergs/cm^2s or 4.4 ergs/cm^2s. However, this connection does not mean causation. There were several instances in which those energy flux values were modelled by OVATION Prime but were not associated with SAPS occurrences. Yet again, one cannot look solely at modelled energy flux data and pinpoint SAPS occurrences. The location of where these energy flux values occur tells a more important story. In 18 of the 87 SAPS events, 20.7 percent, exhibited a clear band of increased energy flux delineating the aurora borealis, referred to as the auroral band. Of these 18 cases, 15 (83.3 percent) exhibit a secondary elevated energy flux value equatorward of the auroral band and are associated with energy flux

values of 3.6 ergs/cm^{2}s and 4.4 ergs/cm^{2}s. In these 15 cases the energy flux values are able to identify and locate the proper magnetic latitude and magnetic local time of the SAPS streamer. Figure 26 shows a clear band of auroral activity extending from 22 MLT through 06 MLT centered around 64 degrees. The red box at 02 MLT and approximately 61 degrees encircles the secondary increase in energy flux which matches the same location of the SAPS streamer.

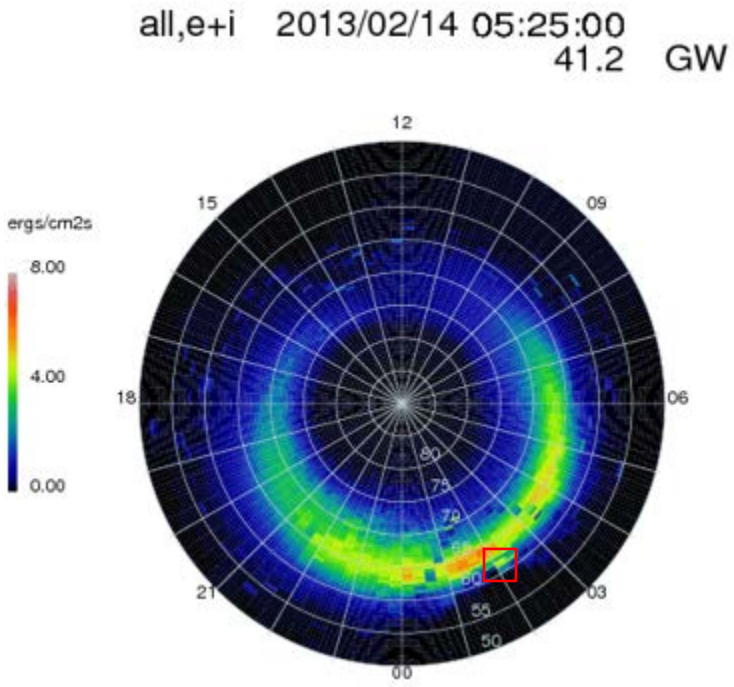

Figure 26 Importance of Energy Flux Location (CCMC)
Highlighting the importance of the location of electron energy flux. The SAPS stream is seen just equatorward of the auroral boundary outlined by the red box. In this instance, the SAPS stream is associated with a total particle energy flux of 4.4 ergs/cm^{2}s. The red box highlights the known SAPS streamer and nicely depicts how the position and location of electron energy flux is just as important as the expected SAPS energy flux value

4.4 Summary

The data shows there is a connection between OVATION Prime's modelled energy flux outputs and known SAPS locations. There is not a magic number that will pinpoint the exact location of the SAPS streamer, but there is a solid connection between the location of the most common energy flux values associated with SAPS events and location of the SAPS streamer. 83% of the cases that had a clearly defined aurora band on the OVATION Prime output and had the expectation value of energy flux just equatorward of the aurora band properly located the plasma flow associated with SAPS.

When the SAPS flow velocity was plotted against particle energy flux there was an exponentially decaying relationship, although there is only slight confidence in this relationship due to the unimpressive R squared value. However, it can be seen that the faster SAPS velocities were associated with a lower particle energy while the slowest SAPS velocities were associated with higher particle energy values. It is surmised that the connection to the model is dependent upon strength of solar activity (geomagnetic storming). It is believed that the stronger storming pushes the sub-auroral activity too far equatorward and out of the area of operation for OVATION Prime. OVATION Prime seems to be a decent tool during moderate storming conditions but seems unreliable when SAPS flow velocities exceed 1,500 meters per second. Despite the noise and high variability of the data, the trends indicate that the particle energy flux still provides information about SAPS maximum flow magnitude even though some data points fall further from the regression line.

5 Conclusions and Recommendations

5.1 Chapter Overview

The primary objective of this study is to develop a method in which OVATION Prime can be used to identify SAPS streamers in order to account for the density trough's impact to HF propagation. The focus is chosen in such a way that would enable Air Force Space Weather Technicians to use current methods and programs to identify and account for impacts from SAPS events. Results from this study can be incorporated into training material to accurately forecast operational HF anomalies.

5.2 Investigative Questions Answered

1. What are the existing abilities by which SAPS are detected and measured? How can those methods be improved?
    a. Currently, SAPS are identified and measured by spacecraft such as the DMSP, as well as Millstone Hill Incoherent Scatter Radar and the SuperDARN radar network. It is possible that SAPS density trough could be detected by an ionosonde, however a density trough does not necessarily mean a SAPS event is occurring. These methods can be improved upon by creating a space physics based mid-latitude ionospheric model that incorporates real-time data to forecast how the ionosphere will evolve overtime. This study has found that under specific conditions, SAPS streamers can be detected on OVATION Prime as a pattern in the particle energy flux.

2. Can the existing space weather technology and forecast methods be adapted or modified to capture SAPS events or associated impacts?
    a. Currently, the Air Force uses the OVATION Prime model to predict auroral clutter. There does seem to be a way to use current solar wind models such as OVATION Prime to identify and capture SAPS events, however it must be under the right circumstances.
3. How will OVATION Prime handle modeling space weather at lower latitudes? Is there a specific limit?
    a. OVATION Prime is best suited being used as an aurora forecast model. However, this study shows that it is not solely limited to aurora forecasting. There are times that it accurately locates SAPS streamers using modeled energy flux, however, it only truly worked on 13 out of 87 cases for an uninspiring 14.9% accuracy. Yes, there does seem to be a specific limit. First off, the OVATION Prime display only covers down to 50 degrees so if impactful space weather occurs equatorward of 50 degrees, it will not be detected by this model. Data trends from section 4 also indicate that the upper SAPS flow limit for OVATION Prime to handle is around 1,500 meters per second.
4. How far equatorward do SAPS typically occur? (How sub-auroral)
    a. An extensive dataset was compiled on 87 SAPS events, to include the minimum and maximum magnetic latitude of occurrence, the numbers show the mean minimum magnetic latitude occurs at 59.55 degree and

the maximum magnetic latitude occurs at 63.69 degrees. Both the mean minimum and the mean maximum latitudes fall within the scope of OVATION Primes output window. There are extreme cases during severe geomagnetic storming that pushes SAPS well beyond the scope of OVATION Prime; the furthest equatorward a SAPS streamer is identified in this study occurs at

5. Is there a temporal dependence on SAPS? (i.e. Seasonal? solar cycle peaks?)
    a. Histogram of monthly occurrence suggests late winter/early spring is the most common time for SAPS to occur. Similarly, 37 events are identified during solar minimum, while the other 50 are seen to occur during solar maximum. SAPS are most likely to occur during solar maximum; this is logical as SAPS is triggered by geomagnetic storming, which increases during solar maximum.
6. Under what conditions can SAPS best be detected in OVATION Prime?
    a. The best regression fit occurs when plotting electron energy flux vs maximum SAPS flow speed. This suggests that the best parameter to track SAPS on OVATION Prime is using only the electron energy flux. Similarly, the best parameter to detect SAPS on OVATION prime is not a distinct numerical value of energy flux, but rather the location. 83 percent of cases are detected when OVATION Prime displays a clear auroral band and also exhibiting electron energy flux expectation values

7. How much can HF operations be improved upon by identifying SAPS events? Is knowing enough?
    a. Based upon the 13 instances in which OVATION Prime energy flux output successfully identified SAPS events, operators could use those to forecast increased HF impacts. Although, it would simply identify to expect increased clutter and signal degradation. In order to mitigate specific impacts, precise knowledge of plasma density trough is needed to properly adjust signal frequency. The exact process of impact mitigation should be a topic of future research.

5.3 Significance of Research

This thesis has revealed several relevant items about SAPS: a relation that is exponentially decaying to particle energy flux which may change during different portions of the solar cycle, the most common values of energy fluctuations associated with SAPS, a curious predisposition for the vernal equinox, as well uncovering the importance of energy flux location in pinpointing SAPS on OVATION Prime.

First addressed is the decaying relationship between SAPS max speed and particle energy flux. The parameter with the best regressional fit is electron particle flux during solar minimum. This should be the first-look parameter when locating SAPS on OVATION Prime. There are a few conjectures for this underlying decaying relationship. The first being that higher flow speeds are connected to fewer particles, meaning each particle carries more kinetic energy. This is logical as it has been discovered that the fastest

SAPS streamers are associated with the deepest ionospheric density troughs, indicating that fewer particles exists to flow at nearly 1,500 meter per second. A secondary conjecture on the cause of the correlation is that higher flow speed means lighter particles—the electrons—carry more of the energy while heavier particles—the ions—carry the preponderance of energy during the lower speeds events. In two-body collision theory, it is expected that the lighter object will have a faster velocity post collision. Finally, there are assuredly aspects at play that the OVATION Prime model does not capture. Influences from external forces such as gravity, pressure and temperature gradients, and the flow of the neutral wind within the thermosphere could be at play. An interesting point is how the best trendline switches to a power law for total particle energy flux during solar maximum. A speculation for this is more CMEs and energetic proton events occur during solar maximum, injecting more heavy particles into the ionosphere allowing the ions to carry the energy, creating a different relationship than exists between the electron workload.

Secondly addressed is the most common values of energy fluctuations associated with SAPS. It was hypothesized that faster flow events would be associated with higher energy fluctuation values, however this is not the case. The typical SAPS event has only moderate energy flux values, of 3.6, 4.0 and 4.4 $\mathrm{ergs/cm^2 s}$. This is interpreted as SAPS events initially increasing energy values, but then remaining relatively constant. The lower smaller fluctuation indicate the energy is not necessarily changing.

Finally, data analysis suggests finding the right energy flux values in the right place, that is, just beyond the auroral oval, is better than simply locating the most common energy flux values associated with SAPS. Similar to weather radar, red does not solely indicate a

tornado, but rather the shape and morphology of the radar returns are used to determine what is truly happening. This location finding can be seen in DMSP data and in incoherent radar data that SAPS tend to occur on the leading edge of the auroral boundary. Figure 6 shows a SAPS event occurring just three degrees equatorward of the auroral boundary. Finding the average energy flux value in the expected location of a SAPS streamer isolated the event in 83 percent of cases.

5.4 Recommendations for Action

It is recommended that data from this thesis be used to establish a rule of thumb for identifying SAPS on OVATION Prime. A rule of thumb is a principle with broad application that is not intended to be strictly accurate or reliable for every situation. It is an easily learned and applied procedure for approximately making a calculation or determination. The first-look parameter during solar minimum should be electron energy flux, which is best used during quiet sun conditions through Kp index of 5. Data plots are best fit for average SAPS flow, above 300 meters per second and below 1500 meters per second—while the Kp index was not tracked in this study, Huang and Foster (2007) discovered a linear relation to Dst and Kp indices, allowing it to be inferred from SAPS flow values.

The forecasting rule of thumb is as follows: when particle energy flux values of 3.6 to 4.4 ergs $\mathrm{ergs}/\mathrm{cm}^2\mathrm{s}$ are seen two to four degrees equatorward of the auroral oval, nowcast a SAPS event with associated HF impacts. Clutter and shortwave fade forecasts must be forecast as High or Severe. There certainly be Doppler clutter as well as the possibility for total signal loss in which the radar will be rendered ineffective.

5.5 Recommendations for Future Research

During the process of this study an accumulated database of SAPS information and traits has been formed. This dataset adds modernized information about SAPS that can be used to verify and expound on the study conducted by Foster and Vo in 2002 when they investigated the average characteristics and activity dependence of SAPS. Moreover, the focus of this thesis could be repeated with data covering a prolonged period of time, such as over the course of multiple solar cycles. Additionally, a deeper exploration into the seasonal dependence of SAPS needs to occur; specifically uncovering why is the month including the vernal equinox more favorable for SAPS development in contrast to the autumnal equinox. Wang and Lühr (2013) discovered a seasonal variation to SAPS impacts to the plasmasphere, but nothing is noted to show preference to spring over fall.

To better answer the final investigative question "How much can HF operations be improved upon by identifying SAPS events? Is knowing enough?" it is suggested that an area of future research compares known SAPS events in this database to operationally observed radar clutter or shortwave fade events. Perhaps a better connection exists between particle energy flux and actual radar clutter or known signal fading. This would take into account both auroral and sub-auroral events to possibly drive an empirical equation to use for more detailed HF clutter charts and forecasts. Whereas this thesis considered particle energy flux as a parameter to use in SAPS identification. Flux values by themselves revealed a correlation of SAPS max flow speeds proportional to the inverse power of energy flux. This is used as a space weather detection tool; the exact processes that cause this relation are merely speculated. More research could be done into what

specifically drives this relationship. The space physics model used in this study has been selected out of convenience of current usage and does not detect the whole picture of what is truly happening in the middle latitudes during space weather events. SAPS are very intricate and couple multiple sections of the Earth's atmosphere and magnetosphere. Continued efforts must focus on developing complex, reliable ionospheric models for the middle latitudes.

5.6 Summary

Several interesting characteristics of SAPS have been discovered by this study. The information is used to create a rule of thumb to aid in clutter forecasting and improve HF operations. Also recognized are areas of future research; there are always ways to improve radar operations and the way they are employed. Propagation impacts and signal loss will not vanish, it is purely mitigated. This study is only the first step in a long process to fully understand the how the space environment impacts daily life and operations.

6 Appendix

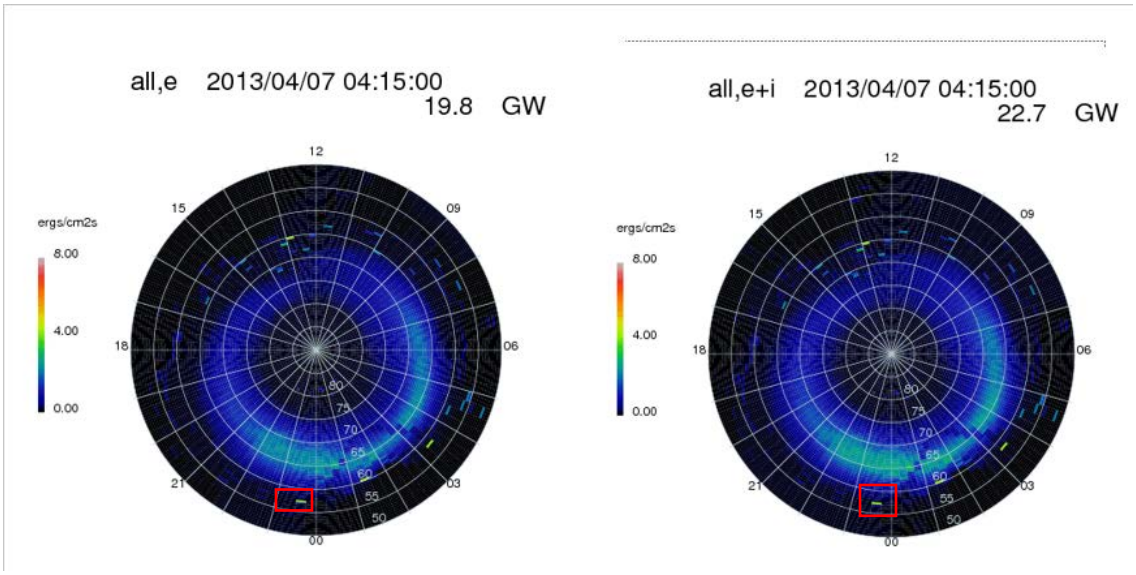

Figure 27 Fastest Westward SAPS Flow on OVATION Prime

OVATION Primes output during the highest magnitude of SAPS event. Westward flow was calculated to be 2,608 m/s. The SAPS stream is located at 2330 MLT at 57 magnetic latitude. Particle energy flux values are 3.6 ergs/cm^{2}s. This is the large outlier seen in Figure 18

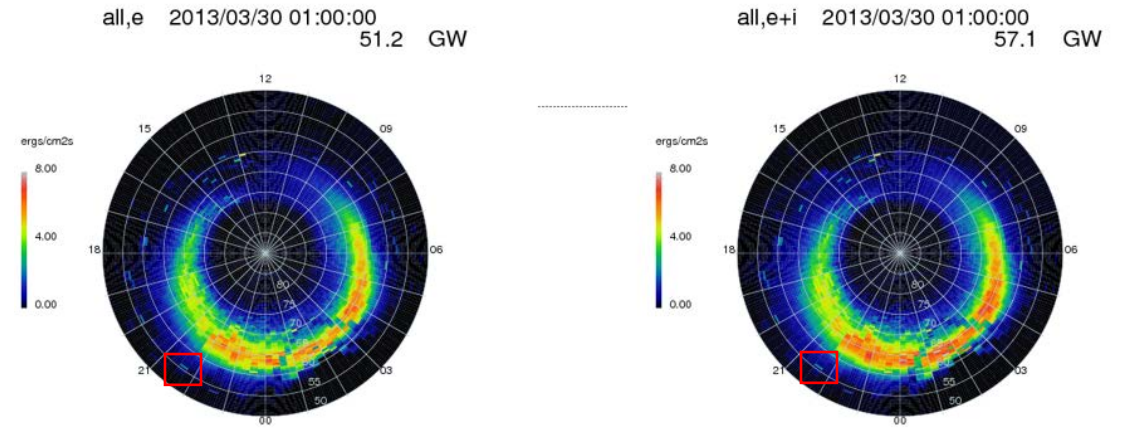

Figure 28 Typical Fast Flow Energy Flux

Common OVATION Prime output during a fast SAPS event. Westward flow was calculated to be 1,923 m/s. The SAPS stream is located 2130 MLT at 51 magnetic latitude. Particle flux values are 1.2 ergs/cm^{2}s for electrons and 1.6 ergs/cm^{2}s for total particle energy flux.

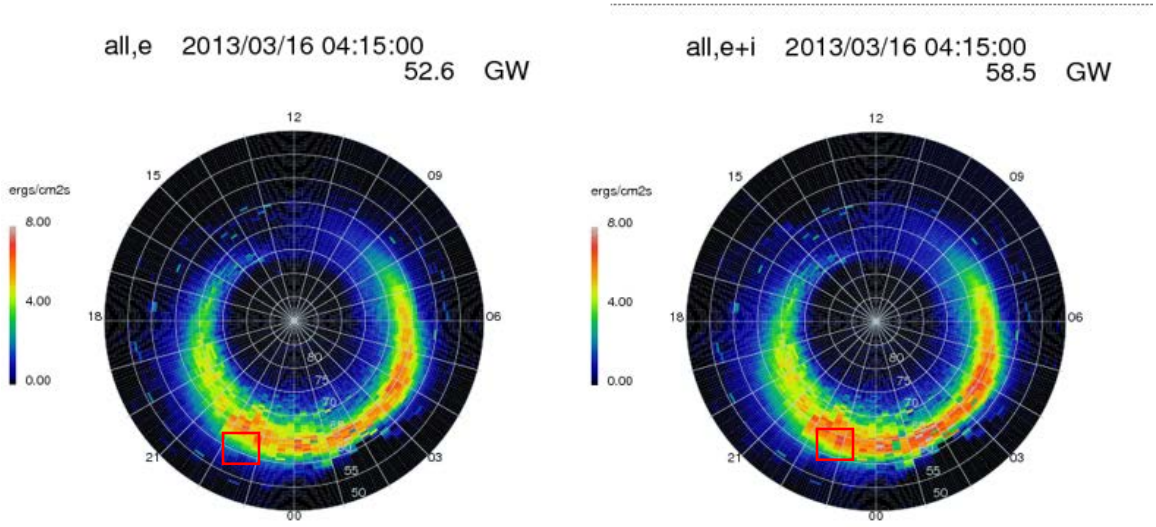

Figure 29 Typical Slow Flow Energy Flux

Common OVATION Prime output during a slow SAPS event. Westward flow as calculated to be 225 m/s. The SAPS stream is located at 2230 MLT at 61 magnetic latitude. This is a low level outlier as the SAPS streamer covered a larger area and did not have a clearly discernable single energy flux value. This could be a source of noise in the data regression fit.

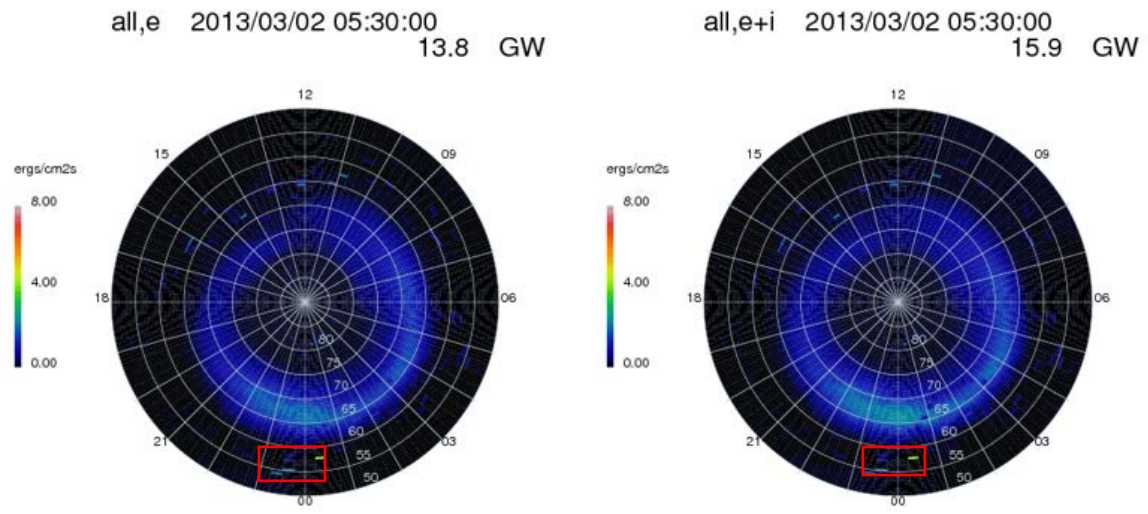

Figure 30 Broad SAPS Stream Identified by Flux Values

This is an outlier as it has the lowest cross polar potential value. However, the SAPS streamer is still noticeable on the OVATION Prime output by picking out the common energy flux values seen poleward of the auroral oval. The SAPS stream is located from 2300 to 0030 MLT at 50 magnetic latitude.

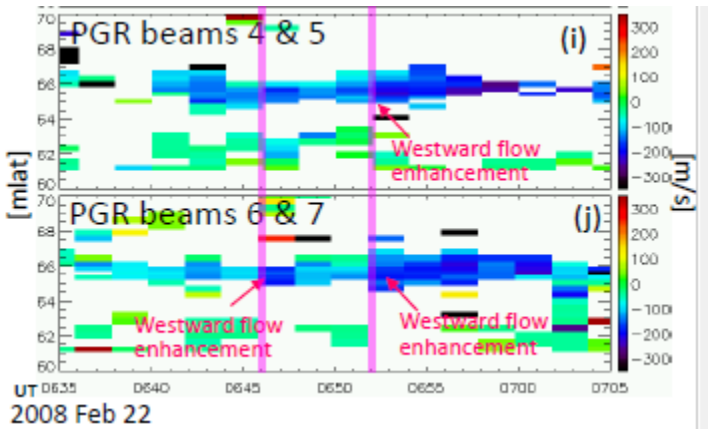

Figure 31 SuperDARN Radar Example

SAPS flow depicted on a radar output. Vertical pink lines show Westward flow enhancement signaling a SAPS event.

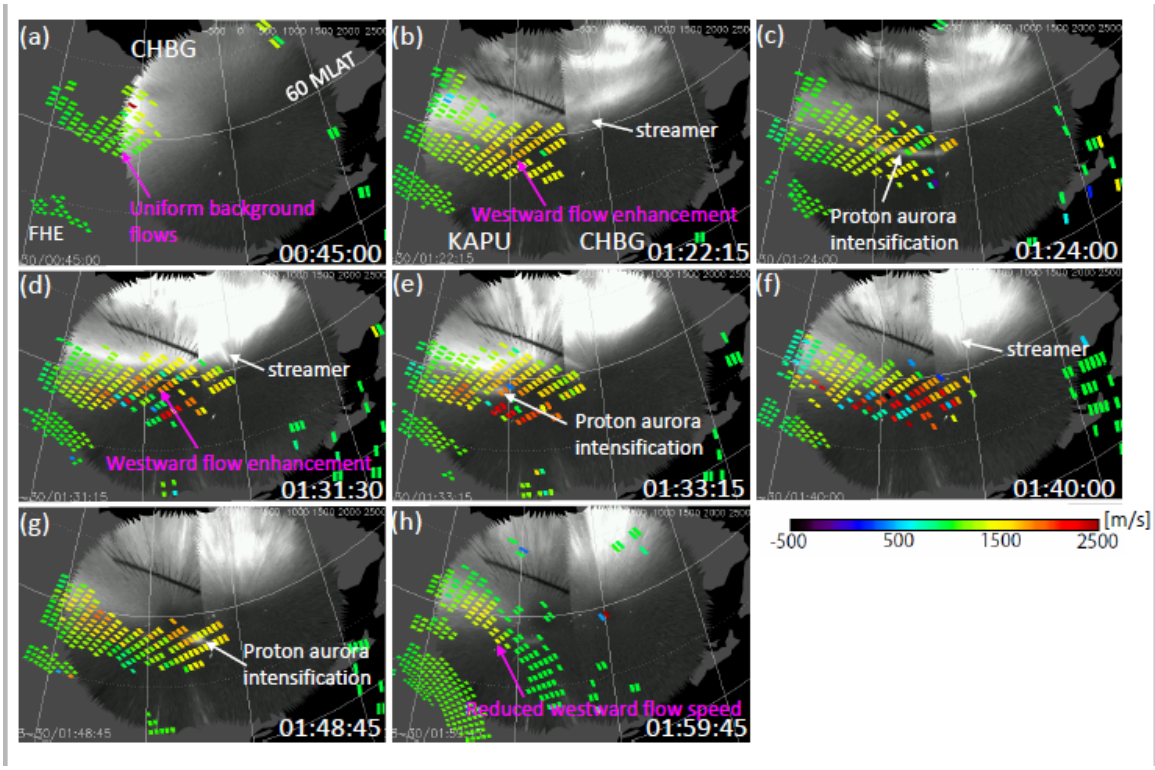

Figure 32 Time Evolution of SAPS Flow

Temporal evaluation of SAPS flow enhancements. Thick black line denotes the auroral boundary and white arrows indicate location of auroral phenomena.

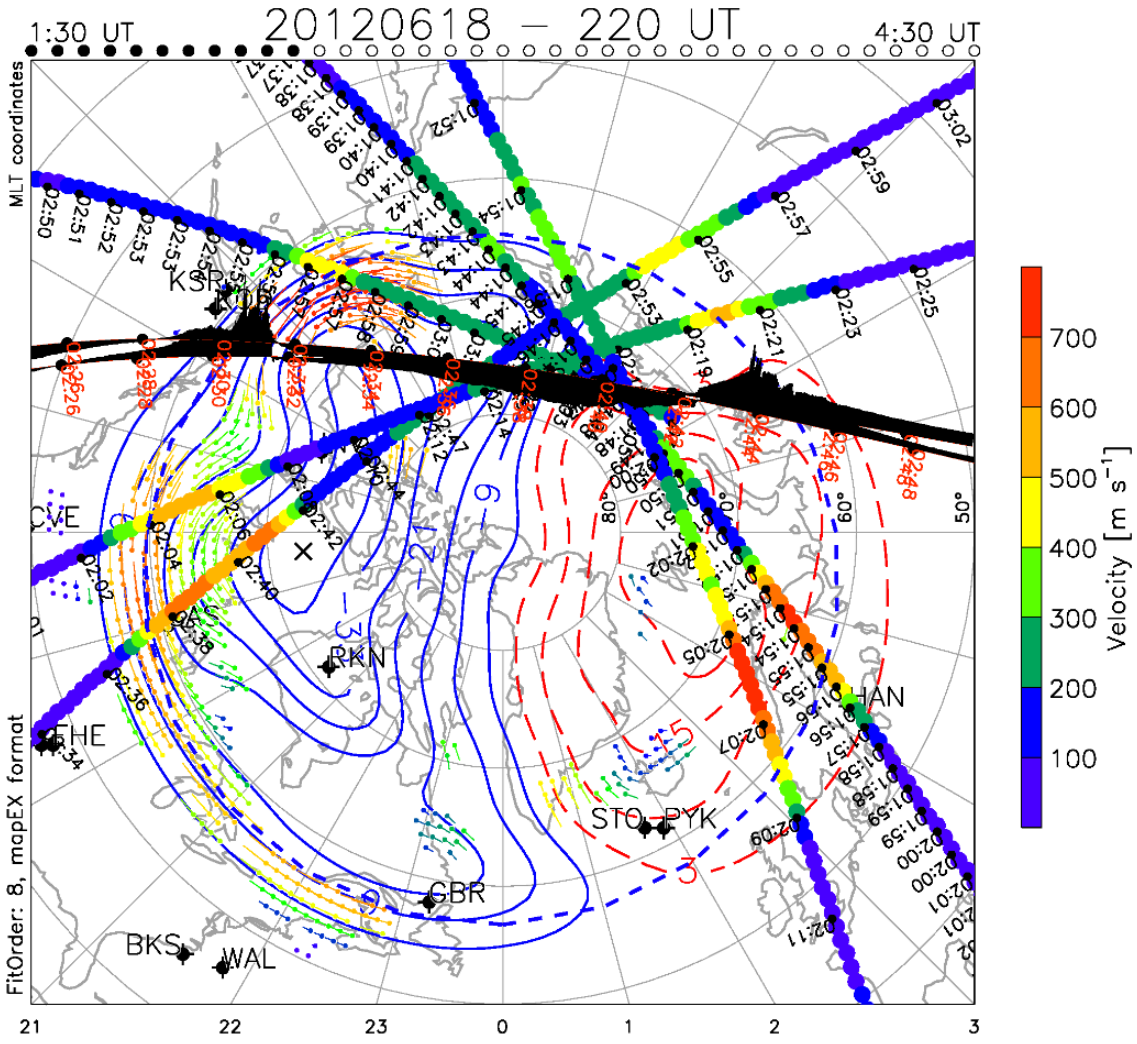

Figure 33 SAPS Observed from Mid-latitude SuperDARN Radar

Observations of SAPS from SuperDARN (dotted colored lines) and different combinations of DMSP Ion Drift Meter (colored cross section passes), AMPERE (solid blue and red lines), and TEC data (thick black line).

year	month	day
2008	2	12
2008	2	12
2008	2	30
2008	2	3
2008	2	4
2008	2	3
2008	2	11
2008	2	10
2008	3	7
2008	3	22
2008	3	24
2008	3	29
2008	3	22
2008	3	29
2008	3	26
2008	4	2
2008	12	15
2009	1	5
2009	2	7
2009	2	24
2009	2	5
2009	2	16
2009	3	14
2009	3	2
2010	1	15
2010	2	17
2010	2	9
2010	2	8
2010	2	4
2010	2	10
2010	2	13
2010	3	2
2010	3	11
2010	4	4
2010	4	24
2010	4	17
2010	4	1

year	month	day
2010	10	15
2010	10	2
2010	10	1
2010	10	15
2010	12	1
2011	2	2
2011	2	1
2011	3	11
2011	3	12
2011	3	16
2011	3	4
2011	4	13
2011	4	16
2011	5	25
2011	5	28
2011	5	16
2011	10	25
2012	1	25
2012	1	7
2012	1	24
2012	3	28
2012	3	13
2012	3	1
2012	4	4
2012	4	13
2012	4	24
2012	4	2
2012	5	23
2012	5	7
2012	5	10
2012	5	4
2012	5	23
2012	6	18
2012	7	10
2012	7	9
2012	8	3
2012	9	2
2012	9	14
2012	11	5
2013	1	4
2013	2	3
2013	3	1
2013	3	15
2013	3	17
2013	3	5
2013	3	30
2013	3	20
2013	3	10

Figure 34 Dates of Identified SAPS Occurrences

Year, month, day of SAPS identified by SuperDARN radar. Column on the left is data categorized as solar minimum while the right column signifies data classified as solar maximum

7 Bibliography

Anderson, P. C., W. B. Hanson, R. A. Heelis, J. D. Craven, D. N. Baker, and L. A. Frank (1993), A proposed production model of rapid subauroral ion drifts and their relationship to substorm evolution, *J. Geophys. Res*., 98, 6069–6078.

Baker, J. B. H., R. A. Greenwald, J. M. Ruohoniemi, K. Oksavik, J. W. Gjerloev, L. J. Paxton, and M. R. Hairston *(*2007*),* Observations of ionospheric convection from the Wallops SuperDARN radar at middle latitudes, *J. Geophys. Res*., 112, *A01303*, *doi:*10.1029/2006JA011982.

Dandekar, B.S., Buchau, J., Whalen, J.A. and Fougree, P. "Physics of the Ionosphere for OTH Operations" Environmental Research Papers, No 1183, Report Pl-Tr-95-2149. Novemer 9, 1995

Foster, J. C., and W. J. Burke, SAPS: A new categorization for sub-auroral electric fields, Eos Trans. *AGU*, 83(36), 393–394, 2002

Foster, J. C., and H. B. Vo, Average characteristics and activity dependence of the subauroral polarization stream, *J. Geophys. Res*., 107(A12), 1475, 2002

Frank, L. A. *(*1967*),* On the extraterrestrial ring current during geomagnetic storms, *J. Geophys. Res.,* 72*(*15*),* 3753–3767, *doi:*10.1029/JZ072i015p03753.

Gallardo-Lacourt, B., Nishimura, Y., Lyons, L. R., Mishin, E. V., Ruohoniemi, J. M., Donovan, E. F., Angelopoulos, V. & Nishitani, N. *(*2017*).* Influence of auroral streamers on rapid evolution of ionospheric SAPS flows. *J. Geophys. Res: Space Physics,* 122. https://doi.org/10.1002/2017JA024198

Galperin,Y,Y N. Ponomarev, and A. G. Zosimova, Plasma convection in the polar ionosphere, *Ann. Geophys., 309-311, 1974.*

Greenwald, R. A., et al. (1995), DARN/SuperDARN: A global view of high- latitude convection, *Space Sci. Rev*., 71, 763–796

Gurnett D.A and Bhattacharjee A, Introduction to Plasma Physics, with laboratory applications, Print. Cambringe University Press 2005 ISBN 978-0521367301

Harel, M., et al, Quantitative simulation of a magnetospheric substorm to Comparison with observations, *J Geophys. Res., 86,* 2242, 1981.

Headrick, J.M. and Thomason, J.F., "Applications of high-frequncy radar", *Radio Science*, Vol 33, No. 4, Pages 1045-1054, July-August 1998.

Huang, C.-S., and J. C. Foster *(*2007*)*, Correlation of the subauroral polarization streams (SAPS) with the *Dst* index during severe magnetic storms, *J. Geophys. Res.*, 112, *A11302*, *doi:*10.1029/2007JA012584.

Iijima,T, and TA. Potemra, The amplitude distribution of field-aligned currents at northern altitudes observed by Triad, *J Geophys. Res., 81,* 2165, 1976.

Kelley, Michael C. The earth's ionosphere : plasma physics and electrodynamics/ International geophysics series; v. 9 Print. 2009. ISBN 978-0-12-088425-4.

Lane, C.T, Comparative statistical analysis of auroral models, Air Force Institute of Technology, March 2012

Laundal,K J.W. Gjerloev, What is the appropriate coordinate system for magnetometer data when analyzing ionospheric currents? *J. Geophys. Res*. (2014). *doi*:10.1002/2014JA020484

Machol, J. L., J. C. Green, R. J. Redmon, R. A. Viereck, *and* P. T. Newell *(*2012*)*, Evaluation of OVATION Prime as a forecast model for visible aurorae, *Space Weather, 10, S03005, doi:*10.1029/2011SW000746.

Nagano, Hiroki, N. Nishitani, and T Hori. "Occurrence Characteristics and lowest speed limit of subauroal polarization streams (SAPS) observed by the Hokkaido East radar." *Earth, Plants and Space*, 67:126, August 2015

Newell, P. T., T. Sotirelis, and S. Wing (2010), Seasonal variations in diffuse, mono-energetic, and broadband aurora, *J. Geophys. Res*., 115, A03216, *doi:*10.1029/2009JA014805.

Nopper, R.W, and R. L.Carovillano, Polar-equatorial coupling during magnetically active periods, *Geophys. Res. Lett.*, 5,699, 1978.

Pisacane, Vincent L. The Space Environment and Its Effects on Space Systems. Reston, VA: American Institute of Aeronautics and Astronautics, 2008. Print. ISBN 978-62410-353-7

Poppe, Barbara B.; K. P. Jorden *Sentinels of the Sun: Forecasting Space Weather*. Johnson Books, Boulder, Colorado pp 2-3, 2006.

Reinisch, B.W. *et al*., "Ionospheric sounding in support of over-the-horizon radar," in *Radio Science*, vol. 32, no. 4, pp. 1681-1694, July-Aug. 1997.

Schunk, R. W., P. M. Banks, and W. J. Raitt (1976), Effects of electric fields and other processes upon the nighttime high-latitude F layer, *J. Geophys. Res*., 81, 3271–3282

Spiro, R.W, R. A. Heelis, and W B. Hanson, Rapid subauroral ion drifts observed by Atmospheric Explorer C, *Geophys. Res. Lett., 6*,657-660, 1979.

Wang, H., Lühr, H. (2013): Seasonal variation of the ion upflow in the topside ionosphere during SAPS (subauroral polarization stream) periods. - *Annales Geophysicae*, *31*, 9, pp. 1521—1534. *doi*: http://doi.org/10.5194/angeo-31-1521-2013

Yeh, H.-C, J. C. Foster, F J. Rich, and W Swider, Stormtime electric field penetration observed at midlatitude, *J. Geophys. Res.*, *96*, 5707, 1991

REPORT DOCUMENTATION PAGE

Form Approved
OMB No. 074-0188

The public reporting burden for this collection of information is estimated to average 1 hour per response, including the time for reviewing instructions, searching existing data sources, gathering and maintaining the data needed, and completing and reviewing the collection of information. Send comments regarding this burden estimate or any other aspect of the collection of information, including suggestions for reducing this burden to Department of Defense, Washington Headquarters Services, Directorate for Information Operations and Reports (0704-0188), 1215 Jefferson Davis Highway, Suite 1204, Arlington, VA 22202-4302. Respondents should be aware that notwithstanding any other provision of law, no person shall be subject to an penalty for failing to comply with a collection of information if it does not display a currently valid OMB control number.
PLEASE DO NOT RETURN YOUR FORM TO THE ABOVE ADDRESS.

1. REPORT DATE *(DD-MM-YYYY)*	**2. REPORT TYPE**	**3. DATES COVERED** *(From – To)*
22-03-2018	Master's Thesis	May 2016 – March 2018

TITLE AND SUBTITLE

Impacts of Sub-Auroral Polarization Streams on High Frequency Operations as a Function of Modeled Particle Energy Flux

5a. CONTRACT NUMBER

5b. GRANT NUMBER

5c. PROGRAM ELEMENT NUMBER

6. AUTHOR(S)

Smith, Nathan D., Captain, USAF

5d. PROJECT NUMBER

5e. TASK NUMBER

5f. WORK UNIT NUMBER

7. PERFORMING ORGANIZATION NAMES(S) AND ADDRESS(S)
Air Force Institute of Technology
Graduate School of Engineering and Management (AFIT/ENY)
2950 Hobson Way, Building 640
WPAFB OH 45433-8865

8. PERFORMING ORGANIZATION REPORT NUMBER

AFIT-ENP-MS-18-M-097

9. SPONSORING/MONITORING AGENCY NAME(S) AND ADDRESS(ES)
2nd Weather Squadron Offutt AFB, NE

10. SPONSOR/MONITOR'S ACRONYM(S)

11. SPONSOR/MONITOR'S REPORT NUMBER(S)

12. DISTRIBUTION/AVAILABILITY STATEMENT
APPROVED FOR PUBLIC RELEASE; DISTRIBUTION UNLIMITED.

13. SUPPLEMENTARY NOTES
This work is a declared work of the U.S. Government and is not subject to copyright protection in the United States.

14. ABSTRACT

Space weather events can cause irregularities within the ionosphere; in particular, this research examines sub-auroral polarization streams (SAPS), as their accompanying irregularities and effects can degrade high-frequency (HF) signal propagation. It is known that the strongest westerly current drifts delineating SAPS are associated with a deep ionospheric trough, which in turn contaminates HF data with clutter from the non-standard ionosphere. Having a methodology to track and identify these occurrences on current computational architecture would provide operators enhanced situational awareness in knowing to expect degradation in HF processes. This study has discovered a weak, yet significant, exponentially decaying correlation between maximum SAPS flow velocity and electron energy flux. Also examined is overarching characteristics most commonly associated with SAPS events. It has been noted that March is the most common month for SAPS formation, as well as finding electron energy flux for SAPS flow to be 4.0 ergs/cm^{2}s with a best regression during solar minimum. The location of the energy flux is just as important as locating the proper energy flux values. This information established an operational rule of thumb to help radar operators determine when SAPS events will degrade standard radar operations.

15. SUBJECT TERMS
SAPS, OTHR, particle energy flux, OVATION Prime

16. SECURITY CLASSIFICATION OF:			**17. LIMITATION OF ABSTRACT**	**18. NUMBER OF PAGES**	**19a. NAME OF RESPONSIBLE PERSON**
a. REPORT	**b. ABSTRACT**	**c. THIS PAGE**			Dr. Robert D. Loper, AFIT/ENP
U	**U**	**U**	**UU**	82	**19b. TELEPHONE NUMBER** *(Include area code)* (937) 255-3636 x4333 Robert.Loper@afit.edu

Standard Form 298 (Rev. 8-98)
Prescribed by ANSI Std. Z39-18

This page intentionally left blank.

→